QUARTZ CRYSTAL MICROBALANCE STUDIES OF DIMETHYL METHYLPHOSPHONATE SORPTION INTO TRISILANOLPHENYL-POSS FILMS

Joshua D. Kittle

Thesis submitted to the faculty of the
Virginia Polytechnic Institute and State University
in partial fulfillment of the requirements for the degree

Master of Science

in

Chemistry

Approved by:
Alan R. Esker, Chair
John R. Morris
Diego Troya

November 6, 2006
Blacksburg, Virginia

Keywords: Langmuir-Blodgett film, trisilanolphenyl-POSS, chemical warfare agent simulant, quartz crystal microbalance

Report Documentation Page

1. REPORT DATE	2. REPORT TYPE	3. DATES COVERED
06 NOV 2006	**N/A**	**-**

4. TITLE AND SUBTITLE	5a. CONTRACT NUMBER
Quartz Crystal Microbalance Studies Of Dimethyl Methylphosphonate Sorption Into Trisilanolphenyl-Poss Films	5b. GRANT NUMBER
	5c. PROGRAM ELEMENT NUMBER

6. AUTHOR(S)	5d. PROJECT NUMBER
	5e. TASK NUMBER
	5f. WORK UNIT NUMBER

7. PERFORMING ORGANIZATION NAME(S) AND ADDRESS(ES)	8. PERFORMING ORGANIZATION REPORT NUMBER
Virginia Polytechnic Institute and State University	

9. SPONSORING/MONITORING AGENCY NAME(S) AND ADDRESS(ES)	10. SPONSOR/MONITOR'S ACRONYM(S)
AFIT/CIA	11. SPONSOR/MONITOR'S REPORT NUMBER(S)

12. DISTRIBUTION/AVAILABILITY STATEMENT

Approved for public release, distribution unlimited

13. SUPPLEMENTARY NOTES

14. ABSTRACT

15. SUBJECT TERMS

16. SECURITY CLASSIFICATION OF:			17. LIMITATION OF ABSTRACT	18. NUMBER OF PAGES	19a. NAME OF RESPONSIBLE PERSON
a. REPORT **unclassified**	b. ABSTRACT **unclassified**	c. THIS PAGE **unclassified**	**UU**	**83**	

QUARTZ CRYSTAL MICROBALANCE STUDIES OF DIMETHYL METHYLPHOSPHONATE SORPTION INTO TRISILANOLPHENYL-POSS FILMS

Joshua D. Kittle

Abstract

Developing methods to detect, adsorb, and decompose chemical warfare agents (CWAs) is of critical importance to protecting military and civilian populations alike. The sorption of dimethyl methylphosphonate (DMMP), a CWA simulant, into trisilanolphenyl-POSS (TPP) films has previously been characterized with reflection absorption infrared spectroscopy, x-ray photoelectron spectroscopy, and uptake coefficient determinations.[1] In our study, the quartz crystal microbalance (QCM) is used to study the sorption phenomena of DMMP into highly ordered Langmuir-Blodgett (LB) films of TPP. In a saturated environment, DMMP sorbs into the TPP films, binding to TPP in a 1:1 molar ratio. Although previous work indicated these DMMP-saturated films were stable for several weeks, DMMP is found to slowly desorb from the TPP films at room temperature and pressure. Upon application of vacuum to the DMMP-saturated films, DMMP follows first-order desorption kinetics and readily desorbs from the film, returning the TPP film to its original state.

Table of Contents

Table of Contents (cont.)

List of Figures

List of Figures (cont.)

List of Tables

Index of Acronyms

CARC   Chemical agent resistive coating

CWA   Chemical warfare agent

DIMP   Diisopropyl methylphosphonate

DMMP   Dimethyl methylphosphonate

GA   Ethyl N,N-dimethylphosphoro-amidocyanidate (Tabun)

GB   2-Propyl methylphosphonofluoridate (Sarin)

GD   3,3-Dimethyl-2-butyl methyl phosphonofluoridate (Soman)

LB   Langmuir-Blodgett

MDCP   Methyl dichlorophosphate

POSS   Polyhedral oligomeric silsesquioxane

QCM   Quartz crystal microbalance

SAM   Self-assembled monolayer

TCP   Trichlorophosphate

TMP   Trimethylphosphate

TPP   Trisilanolphenyl-POSS

VX   O-Ethyl S-2-(diisopropylamino)ethyl methylphosphonothiolate

Acknowledgements

Chapter 1
Introduction and Background

1.1 Chemical Warfare Agents and Simulants

1.1.1 Historical Background

Defined as chemicals which might be employed because of their direct toxic effects on man leading to temporary injury, permanent injury, or death, modern chemical warfare agents (CWAs) first appeared in World War I in the form of chlorine, phosgene, and mustard gas. Although signatories of the Geneva Protocol of 1925 pledged not to use CWAs in warfare, this did not prevent the continued research and development of more lethal agents. German scientists developed several nerve agents during World War II capable of causing respiratory failure and death in minutes. Labeled with the prefix G for "German", followed by a code letter, these agents included tabun (GA), sarin (GB), and soman (GD). Although several large stockpiles of these agents were created, they were not used by the Germans, who feared reprisal by the Allies. After World War II, recovered German CWAs samples led to continued development of CWAs in the United States and other Allied nations. The V-series nerve agents, a more persistent class of CWAs, were developed by the United States in the 1950's and 1960's. Nerve agents, the most devastating type of CWA because of their toxicity and persistency, have been developed by a number of nations over the last 50 years, and the known worldwide stockpiles of CWAs exceed 50,000 tons.[2]

Although capable of decimating military and civilian populations, CWAs have played a limited role in warfare and terrorist attacks. Chemical weapons did see some use in the Iran-Iraq War of the 1980s in the form of mustard gas and GA-filled bombs.

Iranian casualties numbered in excess of 100,000 soldiers, with over 5,000 of these casualties resulting in death. Further, towards the end of the conflict in 1988, the Iraqi Kurdish village of Halabja was exposed to several CWAs, resulting in the death of 10% of the village's 50,000 residents. Several terrorist groups are also known to have pursued the acquisition of CWAs, though to date, only the Aum Shinrikyo group has been successful in using CWAs against civilian populations. This attack occurred in 1995, in which GB was released into the Tokyo subway system, killing 12 and injuring over 5,000.

The destructive and non-discriminating nature of CWAs has led to recent attempts by world bodies to curtail development and destroy existing stockpiles of these agents. The Chemical Weapons Convention of 1993 outlaws the production, stockpiling, and use of CWAs.[3] This arms control agreement has been signed by over 170 nations, though some nations known or suspected of pursuing active CWA programs have refused to ratify the agreement. However, Russia and the United States, with over 42,000 and 25,000 tons of CWAs, respectively, have begun the arduous process of decomposing these agents, though optimal decomposition mechanisms have yet to be developed.

With the push towards demilitarizing chemical weapons, as well as the importance of quickly detecting and decomposing CWAs employed against troops and civilians, research must focus on the bulk reactivity of CWAs as well as their surface chemistry. A thorough understanding of the reaction pathways of CWAs will aid in the development of CWA sensors, environmentally friendly decomposition mechanisms, and improved protective coatings for military personnel and equipment.

1.1.2 CWA Chemistry and Reactivity

The structures of some of the more common CWAs are shown in Figure 1.1; the physical and toxicological properties of these CWAs are shown in Table 1.1.   Few studies have been published concerning the reactivity of CWAs because of the danger of conducting such experiments, the limited laboratory supply of CWAs, and the classified nature of the materials.
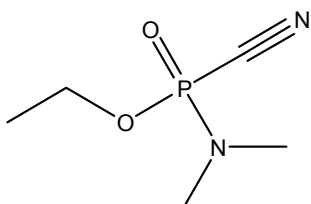
Ethyl N,N-dimethylphosphoro-amidocyanidate (Tabun, GA)
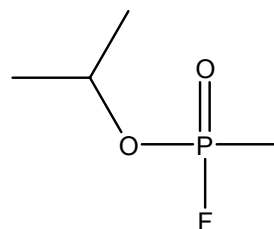
2-Propyl methyl phosphonofluoridate (Sarin, GB)
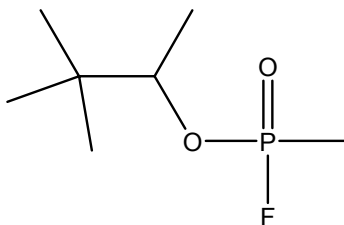
3,3-Dimethyl-2-butyl methyl phosphonofluoridate (Soman, GD)
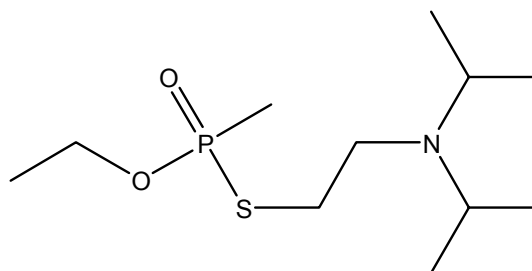
O-Ethyl S-2 (diisopropylamino)ethyl methylphosphonothiolate (VX)

Figure 1.1 Structures of common chemical warfare agents.

Table 1.1 Physical and toxicological data of common CWAs.

Name	Agent Type	Molecular Weight (g/mol)	Boiling Point (°C)	Melting Point (°C)	Vapor Pressure (Torr)*	Decomposition Temperature (°C)	Death by Inhalation (mg-min/m³)
Tabun (GA)	Nerve	162.1	240	-5	0.04	150	135
Sarin (GB)	Nerve	140.1	158	-56	2.9	150	70
Soman (GD)	Nerve	182.2	198	-42	0.4	130	70
VX	Nerve	267.4	240	-50	0.0007 @ 20 °C	36 hr $t_{1/2}$ @ 150 °C	30

* at 25 °C

Baier *et al.*[4] used IR to study the decomposition of GB vapor over Al_2O_3. His results indicated that GB thermally decomposed via a dealkylation reaction to form propylene and methylphosphonofluoridic acid according to the mechanism shown in Figure 1.2.
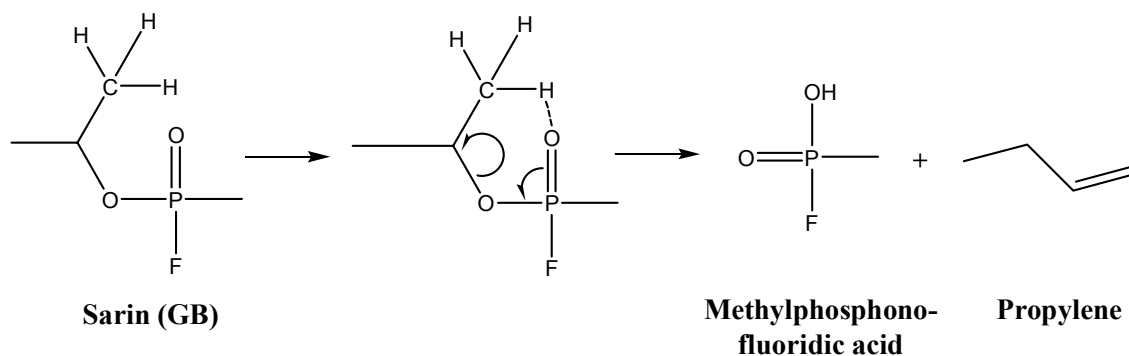
Figure 1.2 The thermal decomposition of GB over Al_2O_3 to methylphosphonofluoridic acid and propylene.[4]

Yang reviewed the solution-phase chemistry of GB, GD, and VX decontamination systems.[5] All three CWAs are rapidly detoxified with bleach solutions, though the solubility of VX drops significantly at high pH and thus requires a 10:1 molar ratio of bleach to oxidize 1 mole of VX. GB and GD dissolve in water and, at pH values

above 10, they hydrolyze in minutes to their respective phosphonic acids, as shown in Figure 1.3. VX also dissolves in pure water, but as the reaction proceeds, the solution becomes more basic and the solubility decreases. Further, as shown in Figure 1.4, one of the reaction pathways forms an extremely toxic compound "EA-2192". However, aqueous solutions of VX can be safely decomposed via oxidation of sulfur and the subsequent hydrolysis of the P-S bond. Several commercial oxidants containing the active species $KHSO_5$ have successfully detoxified large quantities of VX.[6]

GB: R = $(CH_3)_2CH$
GD: R = $(CH_3)CCH(CH_3)$
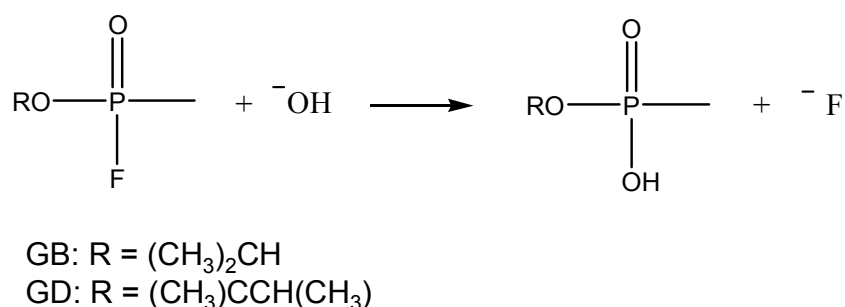
Figure 1.3 Hydrolysis of GB and GD in aqueous solutions at pH > 10.[5]

VX

87%

13%
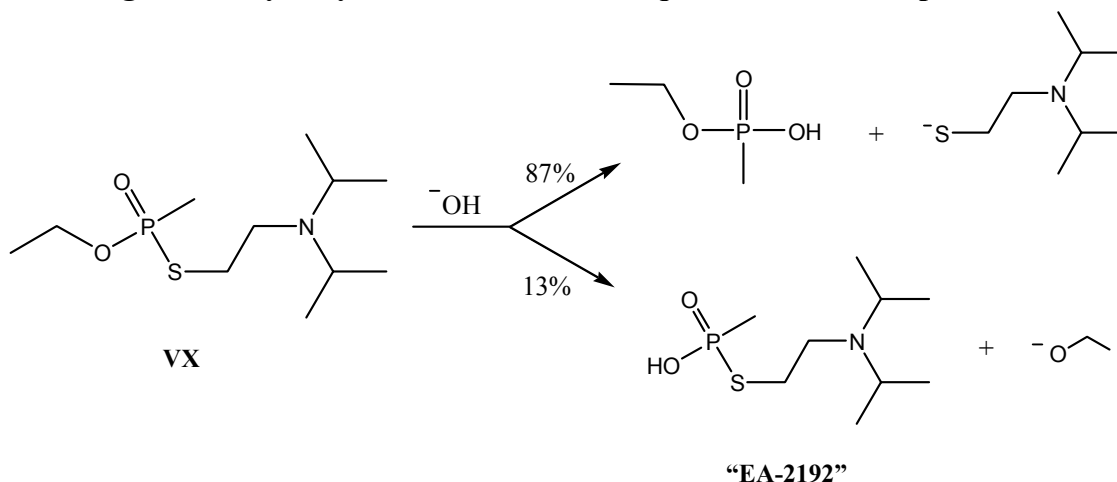
"EA-2192"

Figure 1.4 VX hydrolyzes to primarily form a phosphonic acid and the highly toxic compound EA-2192.[5]

Wagner *et al.* explored the condensed phase chemistry of VX and GD on nanosize MgO,[7] CaO,[8] and Al$_2$O$_3$ [9] with the aid of NMR. Each metal oxide hydrolyzed the CWA, resulting in surface-bound phosphonate products, as shown in Figure 1.5 for MgO and CaO. Although Al$_2$O$_3$ yielded similar products as the other two oxides, it was found to be more reactive than MgO and CaO because the reaction was not surface limited and continued to the core of the of the alumina particles. Wagner also found that the decomposition of VX and GD over the metal oxides was similar to that described by Yang, save that the phosphonate products were bound to the oxide surface and that the hydrolysis of VX did not lead to the formation of the toxic "EA-2192".
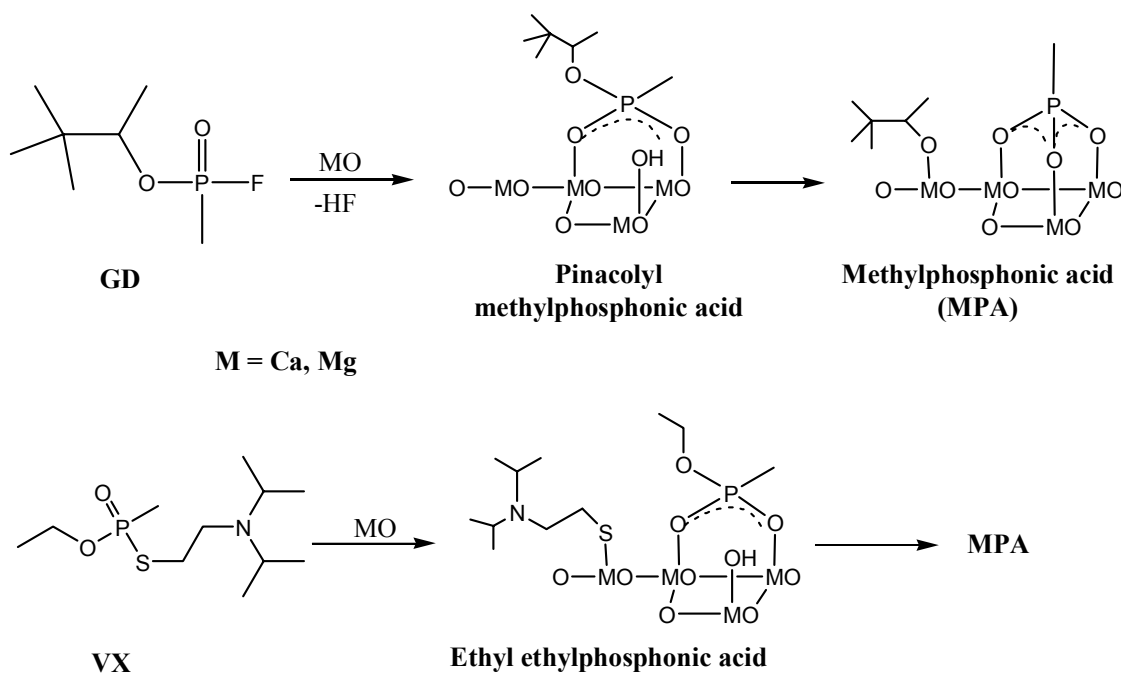
Figure 1.5 Hydrolysis of GD and VX on metal oxides of MgO and CaO. The toxic product EA-2192 was not observed in the hydrolysis of VX over the metal oxides.[9]

1.1.3 CWA Simulant Chemistry and Structures

The inherent toxicity and limited laboratory supply of CWAs has led to the development and study of safer compounds that simulate the chemistry and the reactivity of CWAs. Several of the more common CWA simulants are shown in Figure 1.6; their physical properties are listed in Table 1.2.

Although studies have shown that CWA simulant compounds do not behave identically to the CWA they are intended to mimic, the careful selection of a simulant allows a particular property of a CWA to be studied.[5,10] For example, the reactivity of the halogenated simulants methyl dichlorophosphate (MDCP) and trichlorophosphate (TCP) would more closely imitate the reactivity of GB and GD than the non-halogenated simulants such as dimethyl methylphosphonate (DMMP). However, MDCP and TCP pose more significant health risks than DMMP, and are therefore less frequently studied.

Dimethyl methylphosphonate (DMMP)

Diisopropyl methylphosphonate (DIMP)

Trimethylphosphate (TMP)

Methyl dichlorophosphate (MDCP)

Trichlorophosphate (TCP)
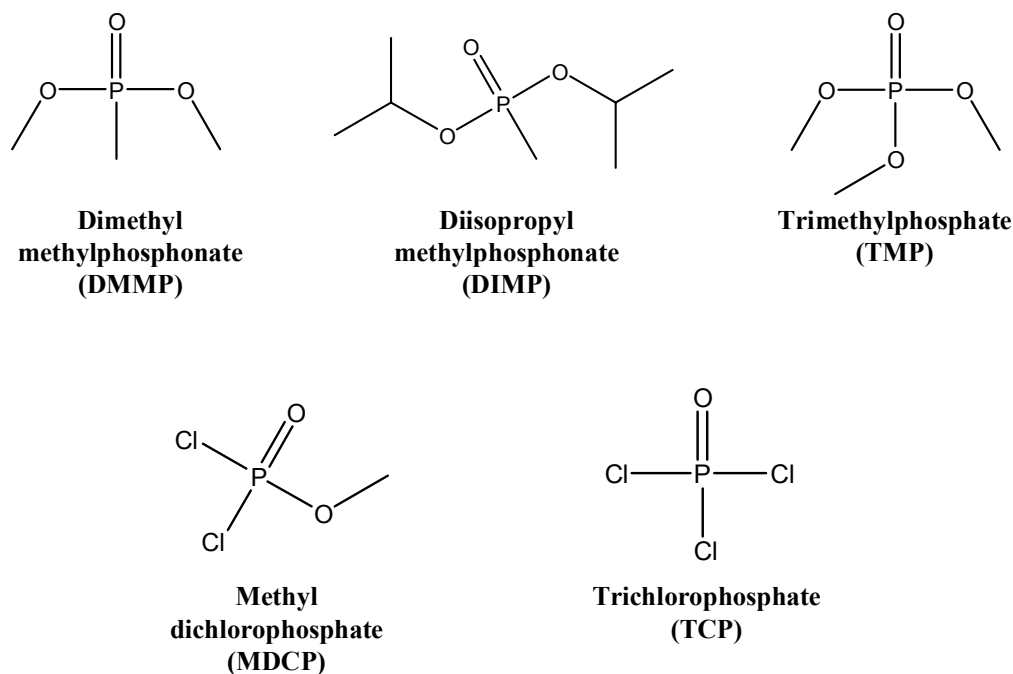
Figure 1.6 Structures of the most commonly studied CWA simulant compounds.

The reactivity of CWA simulant molecules has been studied on a variety of surfaces. DMMP, the most commonly studied CWA simulant, has been reacted over metal oxides,[11-35] self-assembled monolayers (SAMs),[36-40] and polyhedral oligomeric silsesquioxane (POSS) films.[1]

Table 1.2 Physical properties of common CWA simulants.

Name	Molecular Weight (g/mol)	Boiling Point (^oC)	Melting Point (^oC)	Vapor Pressure (Torr)*
DMMP	124.1	181	-	0.962
DIMP	180.2	-	25	0.277
TMP	140.1	197	-46	-
MDCP	148.9	63	-	-
TCP	153.3	106	1.25	-

*at 25 ^oC

On Al_2O_3,[11,12] MgO,[21-26] and TiO_2,[30,31] DMMP adsorbs molecularly: the P=O bond binding with surface acid sites. As temperature is increased, DMMP decomposes, losing methoxy groups to form surface-bound methylphosphonate species. Over Fe_2O_3, DMMP also adsorbs molecularly - as the temperature rises the methoxy groups are driven off. Further, the methyl group is oxidized, an occurrence attributed to the multiple oxidation states of iron. Above 227 °C, all carbon containing species are driven from the iron oxide. Above 377 °C, the phosphorus moves into the bulk, allowing further DMMP adsorption at the surface.[16,17] Unlike the metal oxides, DMMP does not decompose over dehydrated SiO_2 surfaces. Rather, DMMP adsorbs molecularly to surface silanol sites. As the temperature is raised above 300 °C, the DMMP desorbs, restoring the SiO_2 surface to its original state.[27-29]

The adsorption of DMMP has also been studied on methyl, hydroxyl, and carboxylic acid terminated thiol SAMs.[38,39] Weak DMMP adsorption occurs on the methyl terminated SAM, as the methyl groups interact weakly through van der Waals

forces with the alkyl groups of DMMP. The hydroxyl terminated SAM is found to bind multiple layers of DMMP to the surface; the first DMMP layer adsorbs to the surface via hydrogen bonding, while subsequent layers form through van der Waals interactions with other DMMP molecules. Strong DMMP adsorption onto carboxylic acid terminated SAMs also occurs through hydrogen bonding with additional layers forming via van der Waals interactions. Humidity increases the amount of DMMP adsorption on the hydroxyl SAM because an extensive hydrogen bonded network forms. However, DMMP adsorption decreases on the carboxylic acid SAM, as the carboxylic acid is a strong Lewis acid and firmly binds water to the surface, reducing the available hydrogen bonding sites for DMMP.

DMMP also interacts with trisilanolphenyl polyhedral oligomeric silsesquioxane (POSS) films.[1] Under a saturated environment, DMMP adsorbs molecularly to the silanols of trisilanolphenyl-POSS through hydrogen bonding with the phosphoryl oxygen and methoxy groups. Studies indicate that some DMMP remains in the film, even after storage for several weeks. Molecular desorption of DMMP occurs at 154 °C, restoring the POSS film to its original condition.

For all three surfaces – metal oxide, SAM, and POSS, DMMP initially bonds with the surface via bonding through the phosphoryl oxygen. The most significant difference between DMMP and Sarin (GB) is the replacement of a methoxy group of DMMP with a more reactive species – a phosphoryl fluorine. Consequently, the relative safety and lower expected reactivity of DMMP makes it the most widely studied CWA simulant and the simulant used in this work. Thus, the following review of CWA studies will focus primarily on the reactions of DMMP.

9

1.2 CWA Simulant Interactions with Metal and Semi-Metal Oxides

The interaction of metal oxides and CWA simulants has been extensively studied because organophosphonates have demonstrated an ability to adsorb and decompose on metal oxides. Moreover, metal oxides have a high surface area with many reactive sites, and are typically well-defined surfaces. Although the reactivity of CWA simulants has been studied on over fifteen metal oxides, only the five most commonly studied inorganic oxides are reviewed here – aluminum oxide,[11-15] iron oxide,[16-20] magnesium oxide,[13, 21-26] silicon oxide,[27-29] and titanium oxide.[13, 30-35] Although the following review is by no means exhaustive, it does serve to clarify the reactivity of the functional groups of DMMP.

1.2.1 Aluminum Oxide: Interaction with DMMP

Templeton and Weinberg first studied the ability of Al_2O_3 to adsorb CWA simulants.[11,12] The reaction of DMMP with Al_2O_3 over a range of temperatures was followed using inelastic electron tunneling spectroscopy. At -73 °C, DMMP molecularly adsorbed to the surface and saturation occurred at exposures less than 300 Langmuirs. The DMMP behaved as a Lewis base and complexed with surface hydroxyls on the Al_2O_3. Between 2 °C and 200 °C, saturated coverage occurred at exposures lower than 10 torr·s (one Langmuir is equal to 10^{-6} torr·s). Here, the DMMP dissociatively adsorbed to unsaturated aluminum sites, resulting in the cleavage of the phosphorus-oxygen bond and the formation of methyl methylphosphonate (MMP) at the surface. The methoxy fragments formed during this reaction remained covalently bound to the surface at low temperatures. This reaction is depicted in Figure 1.7. Above 300 °C, the MMP decomposed to form a tridentate methylphosphonate species and methanol vapor.
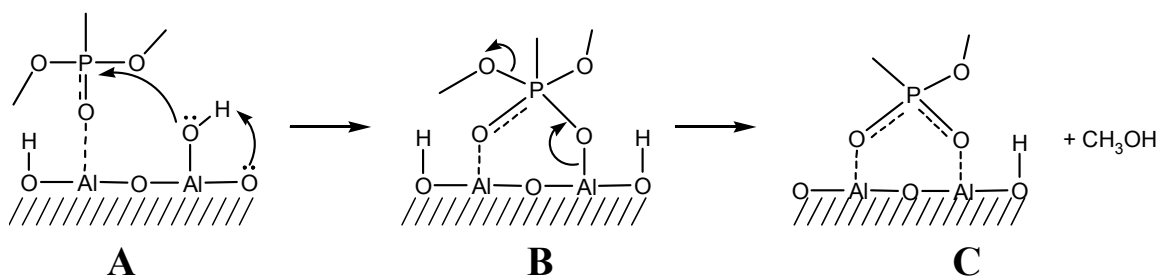
Figure 1.7 The adsorption of DMMP onto Al₂O₃ as presented by Templeton and Weinburg.[11] A) Between 2 °C and 200 °C, DMMP dissociates via cleavage of the phosphorus-oxygen bond. B) Nucleophilic attack by a lattice oxygen occurs at the phosphorus to form a pentacoordinate intermediate. C) A bridged phosphonate product forms on the surface. Methoxy groups are present on the surface at lower temperatures.[11]

Aurian-Blajeni used FTIR to verify Templeton's conclusion that DMMP adsorbs to the Al_2O_3 surface via a phosphorus-oxygen bond. Further, Al_2O_3 was determined to be ineffective as a catalyst for decontamination, as the species irreversibly adsorbed.[13] Mitchell *et al.* also studied the reaction of DMMP on alumina between 25 °C and 400 °C and observed decomposition products in agreement with Templeton.[14] The amount of DMMP adsorbed by commercial Al_2O_3, as well as sol-gel prepared alumina, was also quantitatively determined using FTIR. Commercial Al_2O_3 had a 117 μmol/g capacity at 100 °C, while sol-gel alumina adsorbed nearly double that at 208 μmol/g. The capacity for each tripled at 200 °C and above.[15]

1.2.2 Iron Oxide: Interaction with DMMP

The adsorption of DMMP onto Fe_2O_3 behaves differently than other metal oxides, such as Al_2O_3 and MgO, presumably because of the multiple oxidation states of iron.

Henderson *et al.* studied the interaction of DMMP with Fe_2O_3 surfaces over a range of temperatures using temperature programmed desorption (TPD) and Auger electron spectroscopy.[16] At temperatures below -23 °C, DMMP adsorbed molecularly onto the oxide surface via binding between the phosphorus-oxygen bond and a surface Lewis acid site. Near -23 °C, the methyl group bound to the phosphorous was oxidized by the Fe_2O_3. In addition, the DMMP decomposed to form methoxy groups on the surface and the phosphorus formed bonds with two oxygens present at the oxide surface. At 227 °C, further decomposition resulted in a tridentate-bound adduct and the removal of all carbon-containing species in the form of CO_2, CO, CH_3OH, HCOOH, H_2O, and H_2. Above 377 °C, the phosphorus moved into the bulk of the oxide, which partially restored the surface for further DMMP adsorption and decomposition. These reactions are represented in Figure 1.8.

Mitchell *et al.* also studied the reactions of DMMP with Fe_2O_3, as well as Al_2O_3 and MgO, and observed the same decomposition products as Henderson.[17] IR spectra for the reactions of DMMP over the metal oxides were obtained for a range of temperatures between 25 °C and 300 °C. For Fe_2O_3, Mitchell attributed the easy cleavage of the phosphorus-methyl bond to the multiple oxidation states of iron. As shown in Figure 1.9, the iron oxide surface may serve as an oxidation catalyst through the Mars and van Krevelen mechanism, allowing for a low energy oxidation pathway. Multiple oxidation states are not available for the other metal oxides, possibly explaining why the methyl groups remained bound to the phosphorus.
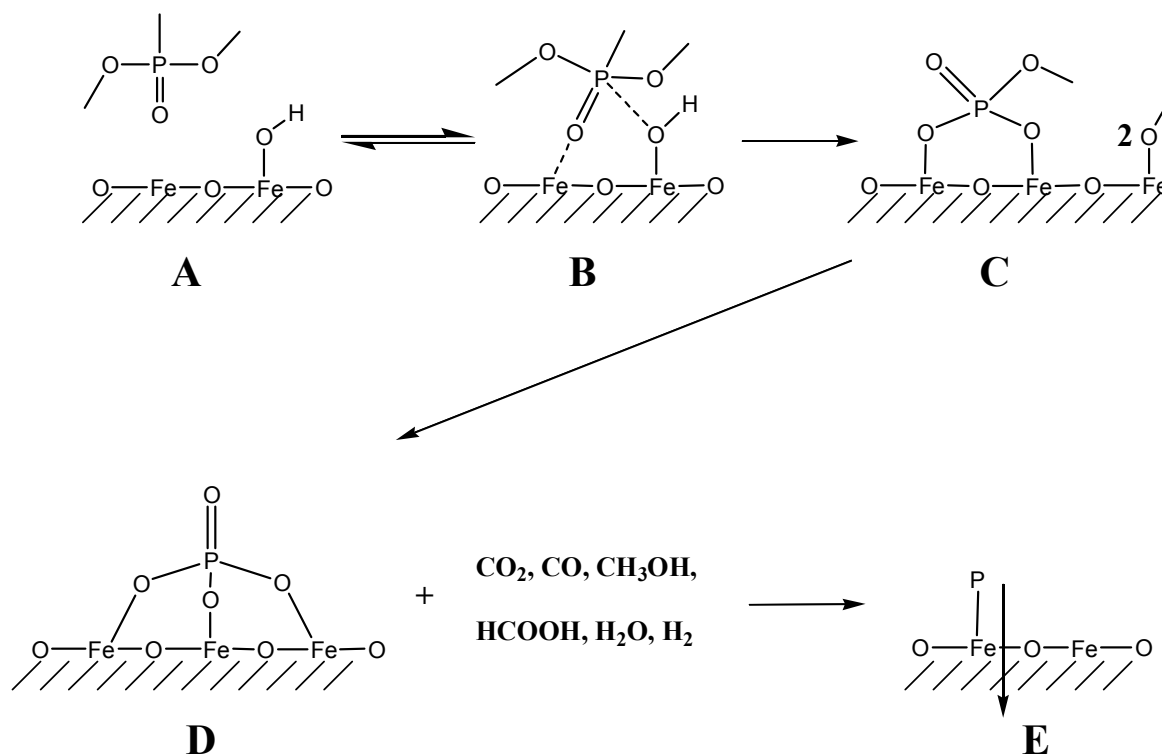
**Figure 1.8 The adsorption and decomposition of DMMP on Fe$_2$O$_3$.
A) DMMP approaches the oxide surface.
B) At -103 °C, DMMP molecularly adsorbs to the surface.
C) At -23 °C, the methyl group is oxidized and DMMP decomposes and bonds to the oxide. D) At 227 °C, the adduct further decomposes to form a tridentate species; all carbon-containing compounds are removed.
E) Above 377 °C, phosphorus moves into the bulk, allowing further DMMP adsorption.[17]**

Mitchell *et al.* also quantitatively determined the amount of DMMP adsorbed onto an alumina-supported iron and cerium oxide surface using FTIR.[18,19] At 25 °C, the alumina-supported oxide surface adsorbed approximately 510 µmol of DMMP per gram of oxide, while aluminum oxide alone adsorbed 317 µmol/g. Temperature affected the amount of adsorption, with increasing temperature resulting in increased adsorption. Klaubunde *et al.* also quantitatively studied the adsorption of DMMP onto metal oxides

and concluded that small amounts of Fe_2O_3 coated on the surface of nanocrystalline metal oxides improved the reaction efficiency when compared to the metal oxides without Fe_2O_3.[20]

$$Fe_2O_3 + 2e^- \longrightarrow 2FeO + O^{2-}$$

$$(H_3CO)_2P(O)\text{-}CH_3 + O^{2-} \longrightarrow (H_3CO)_2P(O)^-_{ads} + H_3CO^-_{ads}$$

$$2FeO + \tfrac{1}{2}O_2 \longrightarrow Fe_2O_3$$
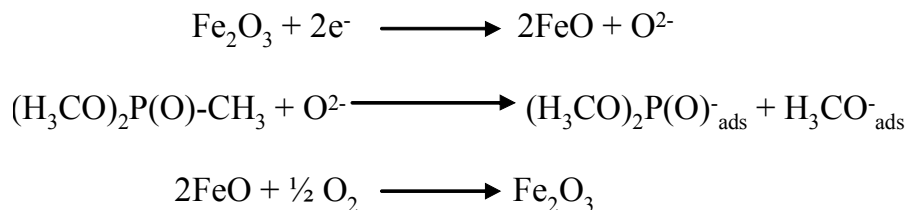
Figure 1.9 Mars and van Krevelen mechanism for the oxidation and decomposition of DMMP on an Fe_2O_3 surface.

1.2.3 Magnesium Oxide: Interaction with DMMP

Klabunde *et al.* probed the interaction of organophosphonates and MgO using a variety of techniques, including FTIR, pulsed microreactors, gas chromatography-mass spectrometry (GC-MS), x-ray photoelectron spectroscopy (XPS), and atomic force microscopy (AFM).[21-26] Their studies indicated that DMMP adsorbed and decomposed over MgO according to the pathway shown in Figure 1.10. At room temperature, DMMP molecularly adsorbed, most likely through the phosphoryl oxygen and a Lewis acid site on the MgO surface, although some DMMP decomposition did occur at room temperature. DMMP decomposition was complete at 190 °C. A surface methoxy group was evolved and an O-P-O bridged species was formed: one of the oxygens was provided by the MgO surface, as proven by an ^{18}O-labeling experiment. Additional DMMP could oxidize the surface-bound methoxy group, generating a surface-bound hydrogen and evolving formic acid, the major decomposition product observed. The deoxygenated DMMP likely adsorbed to the MgO surface, forming a surface methoxy group and also a bridging species in which both oxygens are supplied from the surface. Above 600 °C, the

phosphorus-methyl bond was cleaved; additionally, the formic acid decomposed into carbon monoxide and water.
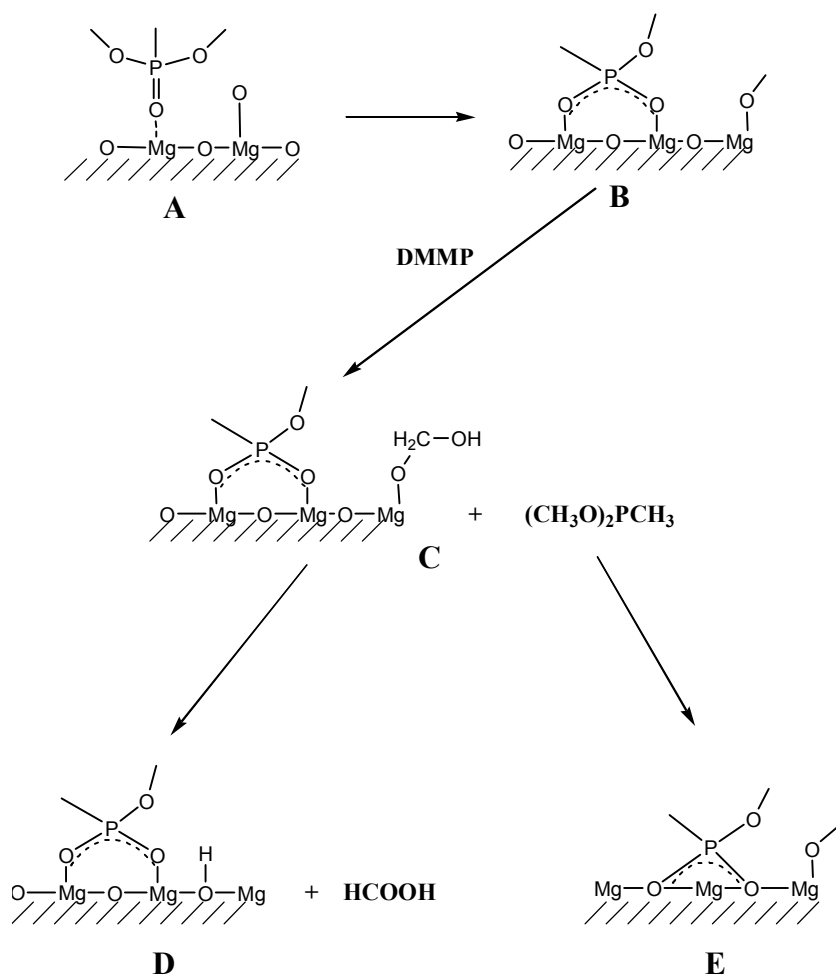
Figure 1.10 Adsorption and decomposition of DMMP onto MgO. A) DMMP molecularly adsorbs to MgO at room temperature. B) DMMP decomposes above 190 °C to form a bridged species and a surface methoxy group. C) Additional DMMP oxidizes the surface methoxy group. D) Formic acid is evolved from the surface.   E) Deoxygenated DMMP forms a bridged species and a surface methoxy group.[22]

Klabunde *et al.* also examined the effect of water on the decomposition of DMMP over MgO.[24] Their results indicated that the presence of water dramatically enhanced the ability of the surface to decompose the DMMP. Also, pulsing water over the surface

partially regenerated the activity of the MgO surface, allowing further decomposition of fresh DMMP. The primary decomposition product in the presence of water was methanol (as opposed to formic acid) because of the abundance of hydrogen species available to protonate the surface-bound methoxy groups.

Aurian-Blajeni and Boucher investigated the gas-solid interaction of DMMP over magnesium oxide using FTIR.[13] Their results also indicated that DMMP initially adsorbed to the magnesium via the P=O bond and decomposed to form methoxy groups. The adsorption and decomposition of DMMP increased with exposure time and surface area. Temperature and vapor pressure also affected the adsorption of DMMP according to an Arrhenius-type equation:

$$q_{t=1h} = cT^{-1/2}exp^{(-E/RT)} \qquad (1.1)$$

$q_{t=1h}$ is the amount of DMMP adsorbed after one hour, c is proportional to the vapor pressure of DMMP, and E is the activation energy.

1.2.4 Silicon Dioxide: Interaction with DMMP

Henderson *et al.* examined the interaction of DMMP with SiO_2 surfaces using TPD and Auger electron spectroscopy.[27] At -103 °C, DMMP molecularly adsorbed to dehydrated SiO_2, forming a multilayer under saturated conditions. By -2 °C, DMMP had desorbed to form a monolayer on the surface. At 300 °C, the monolayer molecularly desorbed according to first order kinetics with an activation energy for desorption of 70.7 kJ/mol. Unlike reactions with the metal oxides, such as aluminum oxide and magnesium oxide, no DMMP decomposition was evident over dehydrated SiO_2.

Henderson *et al.* did observe some DMMP decomposition over extensively hydrated SiO_2 surfaces. In their study with hydrated surfaces at 25 °C, DMMP was

introduced and data was collected over a temperature range of 27 °C to 427 °C. The results for the hydrated and dehydrated silica surfaces were nearly identical, save for the detection of small quantities of methanol and methylphosphonate desorbed from the hydrated surface at 377 °C. The authors attributed these products to the hydrolysis of the DMMP methoxy groups. However, this effect was limited, as the DMMP peak area decreased by only 8-10%; furthermore, the presence of water did not enhance DMMP adsorption to the surface.
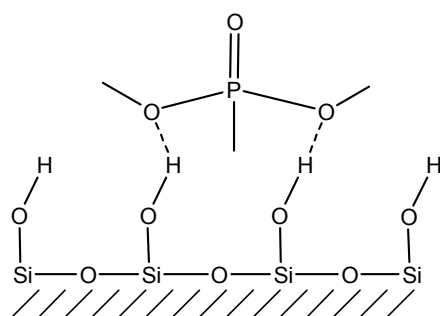
Figure 1.11 Adsorption of DMMP onto SiO$_2$ via hydrogen bonding between surface silanols and the methoxy groups of DMMP.[28]

Kanan and Tripp also studied the reactions of organophosphonates and dehydrated SiO$_2$ using FTIR to monitor DMMP adsorption.[28,29] Their work indicated that DMMP molecularly adsorbed via hydrogen bonding between the methoxy groups and surface silanols, as shown in Figure 1.11. In agreement with Henderson *et al.*, complete molecular desorption occurred by 300 °C, restoring the silica surface to its original condition.

1.2.5 Titanium Dioxide: Interaction with DMMP

Aurian-Blajeni and Boucher first examined the adsorption of DMMP over TiO$_2$.[13] Using FTIR, DMMP was shown to molecularly adsorb to the surface through the P=O bond. However, over the spectral region investigated, DMMP and the likely

decomposition product, methyl methylphosphonate, had identical peaks, prohibiting the resolution of any DMMP decomposition on titanium dioxide. Rusu and Yates, as well as Kim *et al.*, also used FTIR to follow the reactions of DMMP on TiO$_2$ surfaces.[30,31] Below -73 °C, DMMP adsorbed molecularly to the surface through the phosphoryl oxygen, in agreement with Aurian-Blajeni and Boucher. Above -59 °C, the adsorbed DMMP decomposed to methyl methylphosphonate via cleavage of the methoxy groups, which subsequently bound to the titanium oxide surface (Figure 1.12). Thus, the adsorption and decomposition of DMMP over TiO$_2$ is similar to that of other metal oxides, such as Al$_2$O$_3$ and MgO.
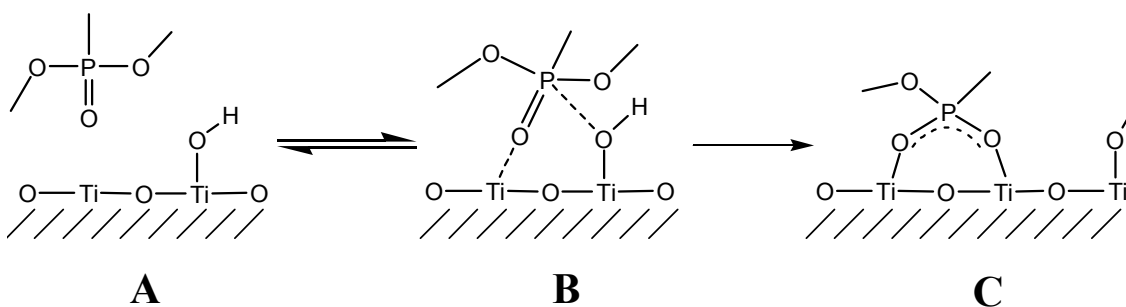
Figure 1.12 Adsorption and decomposition of DMMP onto TiO$_2$. A) DMMP approaches the oxide surface. B) Below -73 °C, DMMP molecularly adsorbs to the surface. C) Above -59 °C, DMMP decomposes to form a bridged methylphosphonate species and surface methoxy groups.[30]

The photocatalytic decomposition of DMMP over TiO$_2$ has also been extensively studied.[32-35] Application of UV light to titanium excites an electron from the valence band to the conduction band. The resulting conduction band electron is capable of reducing species on the surface, while the valence band hole is available to oxidize species. Obee and Satyapal used a single-pass reactor at room temperature to observe the photocatalytic decomposition of DMMP over TiO$_2$ surfaces.[32] Reaction products were

analyzed using a photo-acoustic detector, as well as a gas chromatograph equipped with a flame ionization detector. Their work indicated that the valence band holes cleaved the P-O bonds, followed by eventual P-C bond cleavage. Methyl phosphonic acid, phosphate ions, carbon dioxide, and carbon monoxide were the detected decomposition products. Furthermore, they postulated that hydroxyl attack provided another oxidation pathway for DMMP. As shown in Figure 1.13, hydroxyl radicals may have formed via the reaction of water with surface valence band holes. These hydroxyl radicals could react with DMMP through hydrogen abstraction or addition-elimination pathways to form the observed products. Obee and Satyapal also found that reactivity towards DMMP was completely restored by washing the surface with water. The surface was also partially restored upon UV irradiation. Similar studies following the photocatalytic decomposition of DMMP over TiO_2 conducted in aqueous solutions also yielded methyl phosphonic acid and phosphate ions.[33]

1.3 CWA Simulant Interactions with Organics and Organic Hybrids

Recently, polyurethane films have seen use as chemical agent resistive coatings (CARC) to protect military equipment. In addition, several CWA sensors have been developed that incorporate polymer films to aid in identifying organophosphonates.[41,42] However, few studies have focused on the surface chemistry behind CARCs and polymer-based CWA sensors. The study of the molecular interaction of CWA simulants over well-defined organic and organic hybrid films aids the understanding of existing polymer coatings and may lead to the development of improved organic or organic hybrid coatings.

A)

$$TiO_2 + h\nu \longrightarrow e_c^- + h_v^+$$

$$e_c^- + O_2 \longrightarrow O_2^-$$

$$h_v^+ + H_2O \longrightarrow H^+ + {}^{\bullet}OH$$
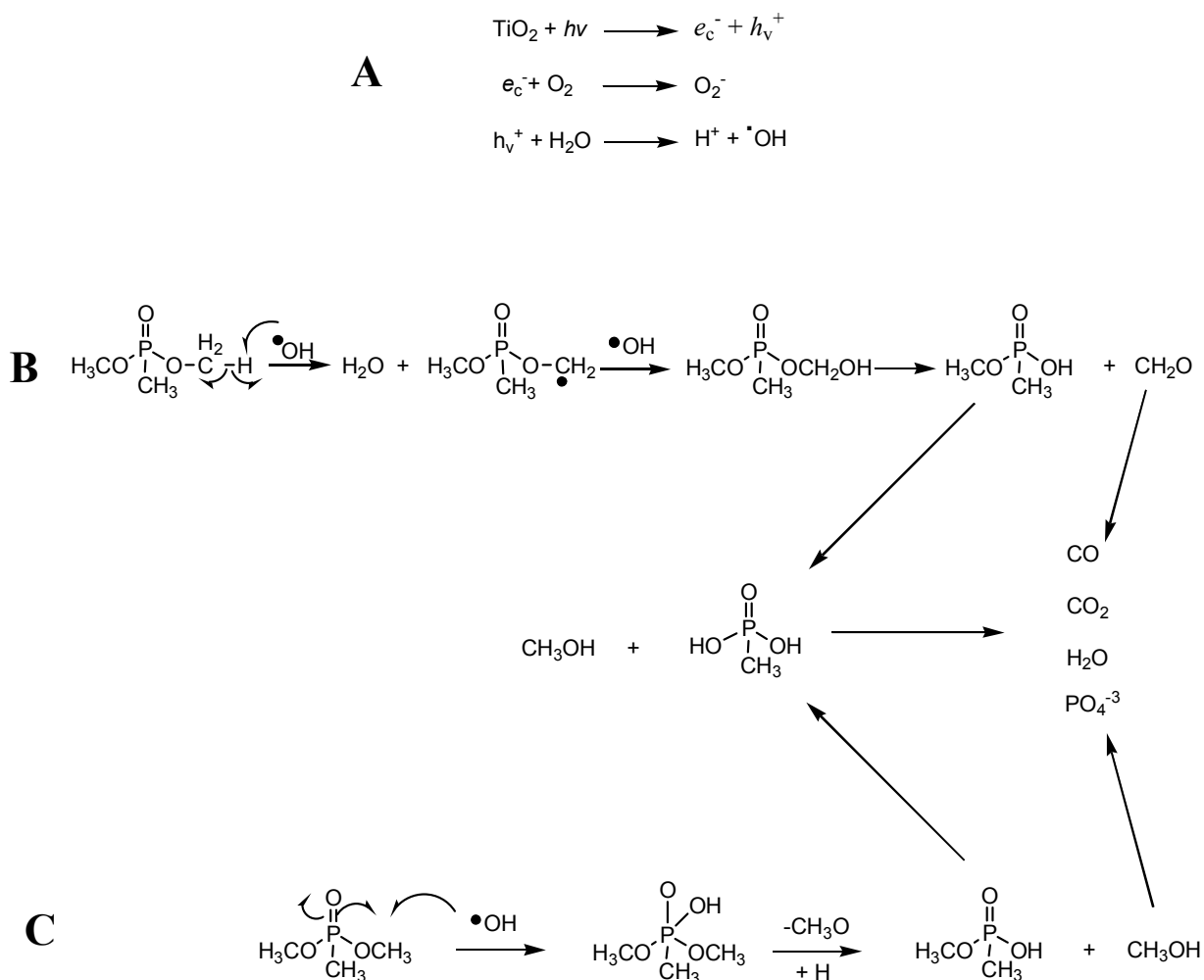
Figure 1.13 **Photocatalytic decomposition of DMMP over TiO$_2$. A) UV light promotes an electron to the conduction band (e_c^-); the valence band hole (h_v^+) reacts with water to form hydroxyl radicals. B) Formation of methyl methylphosphonate, phosphate ions, carbon dioxide, carbon monoxide, and water via hydrogen abstraction. C) Formation of methyl methylphosphonate, phosphate ions, carbon dioxide, carbon monoxide, and water via addition-elimination.[32]**

20

1.3.1 SAMs: Interactions with DIMP and DMMP

Kepley *et al*. first considered the use of a SAM for sensing organophosphonate compounds.[36] They entrained DIMP or DMMP in high-purity N_2 vapor, which was then flowed over a surface acoustic wave (SAW) device containing a SAM/Cu^{+2} monolayer. The SAW was composed of quartz crystals deposited with an Au-on-Cr electrode. An 11-mercaptoundecanoic acid (MAU) SAM was formed on the Au substrate, followed by the addition of copper ions to the end of the MAU chains. Up to 20 layers of the CWA simulants were found to bind to the Cu^{+2}-terminated surface. This reaction was reversible: with the introduction of pure N_2 vapor, 90% of the CWA simulant desorbed in less than two minutes. Crooks *et al*. also used a SAW to examine the ability of an MAU/Cu^{+2} SAM to adsorb DIMP and obtained results in agreement with Kepley *et al*.[37] In addition, their IR results indicated that the first layer of DIMP interacts strongly with the Cu^{+2} surface via the phosphoryl oxygen. The subsequent DIMP layers form a solid-like phase as a result of nucleated growth around the first layer.

Bertilsson *et al*. studied the adsorption of DMMP onto methyl, hydroxyl, and carboxylic acid terminated thiol SAMs using SAW and reflection absorption infrared spectroscopy (RAIRS) at room temperature.[38,39] The methyl-terminated surface weakly interacted with the DMMP, adsorbing less than 0.1 monolayers of DMMP when the initial concentration was 26 ppm. The hydroxyl surface moderately interacted with the DMMP via hydrogen bonding with the phosphoryl oxygen, adsorbing 0.6 monolayers of

DMMP when the initial concentration was 26 ppm. The strongest interaction occurred via hydrogen bonding at the carboxylic acid terminated SAM, which adsorbed 0.7 monolayers when the initial concentration was 26 ppm. Higher concentrations of DMMP led to the adsorption of additional layers on the hydroxyl and carboxylic acid terminated surfaces, attributed to van der Waals interactions between alkyl groups, as shown in Figure 1.14.

Bertilsson *et al.* also studied the effect of co-adsorbed water on the adsorption of DMMP onto methyl, hydroxyl, and carboxylic acid terminated thiol SAMs using SAW and RAIRS.[40] A humid environment did not affect the methyl terminated SAM, as little adsorption of DMMP was observed, in agreement with previous work. However, humidity significantly influenced the hydroxyl and carboxylic acid terminated SAMs: increased humidity led to increased DMMP adsorption for the hydroxyl terminated SAM, while increased humidity led to decreased DMMP adsorption for the carboxylic acid terminated SAM. The hydroxyl SAM interacted with co-adsorbed water and DMMP to form a network of hydrogen bonding composed of bonds with the phosphoryl oxygen of DMMP, reorganized surface hydroxyls, and free hydroxyl groups at the surface. However, the carboxylic acid SAM is a strong Lewis acid and firmly bound pre-adsorbed water to the surface. Consequently, fewer hydrogen bonding sites were available for the adsorption of DMMP. Clearly, water and humidity affect the adsorption of CWA simulants and must be studied in the formation of sensors and decomposition reactions.
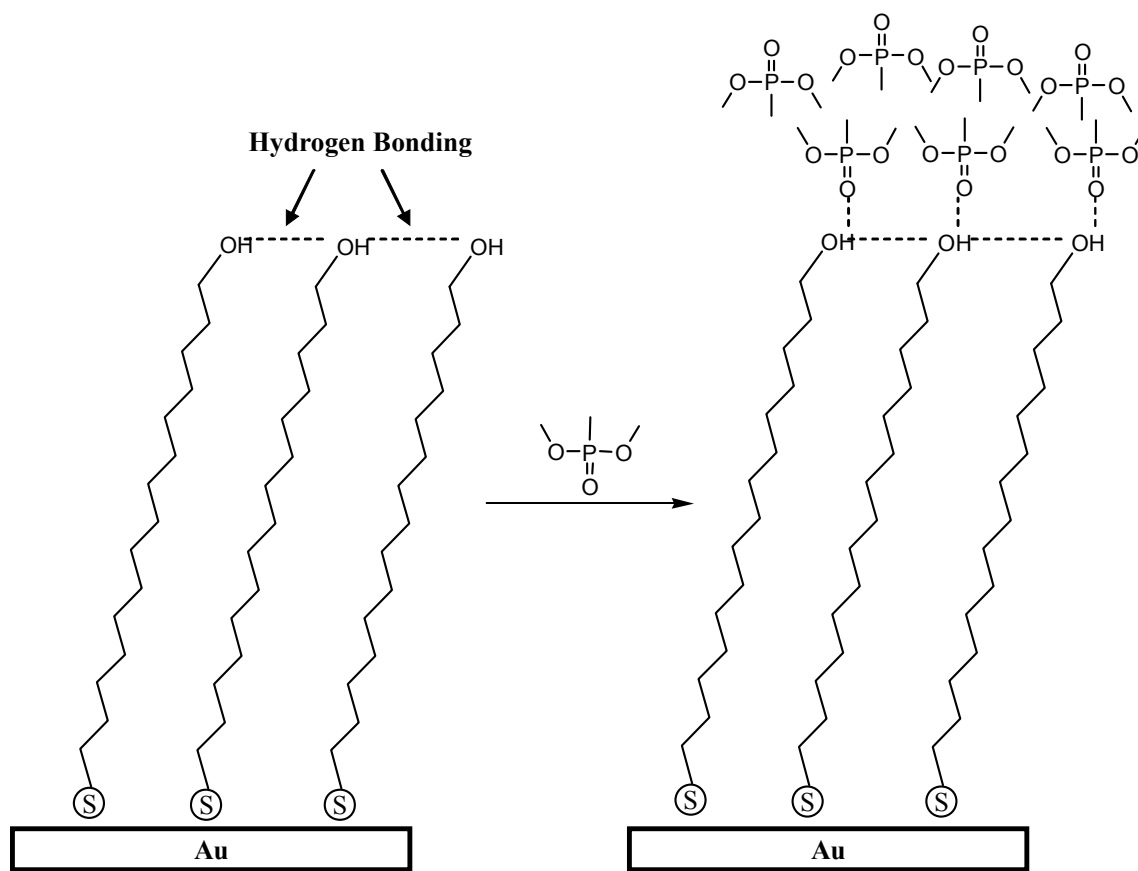
Figure 1.14 Adsorption of DMMP onto a hydroxyl-terminated SAM. The initial DMMP layer binds through hydrogen Bonding, while subsequent layers are weakly held via van der Waals interactions.

1.3.2 POSS: Interaction with DMMP

Ferguson-McPherson *et al.* studied the interaction of DMMP with trisilanolphenyl-POSS (TPP) Langmuir-Blodgett (LB) films through the determination of uptake coefficients, RAIRS, and TPD.[1] Trisilanolphenyl-POSS is composed of a caged silica core and peripheral phenyl groups; one corner of the cage is open and contains three silanol groups, as shown in Figure 1.15. A more detailed review of TPP LB-films is presented in Chapter 3.

Uptake coefficients of DMMP into the TPP films were measured in an ultra high vacuum (UHV) molecular beam scattering chamber. A DMMP/N_2 vapor was formed by

bubbling N_2 at 750 torr through DMMP, a liquid at room temperature, at 80 °C. The resulting molecular beam struck a 1 cm^2 area of the TPP film. By determining the fraction of the incident beam that adsorbed to the surface according to the King and Wells technique,[43] uptake coefficient measurements were recorded at a base pressure of 5 x 10^{-10} torr over a range of temperatures from -123 °C to 25 °C. Because the outer layer of the TPP films is composed of phenyl groups, the sticking probability of DMMP on TPP was found to be ≤ 0.05, which is in agreement with the findings of Bertilsson *et al.* and Crooks *et al.* that DMMP weakly adsorbs to hydrophobic species at room temperature.[38,39]

In spite of the low uptake probability of impinging DMMP molecules, DMMP did sorb into TPP films under saturated conditions as evidenced by RAIRS.[1] TPP films were placed in a N_2 purged, sealed, 60 cm^3 vapor deposition chamber and 5 μL of DMMP was injected. The chamber was heated to 35 °C for 10 minutes. The resulting DMMP saturated film was placed directly into the RAIRS chamber and the spectra was obtained at room temperature under high vacuum. Relative to the pure TPP film, the SiO-H of the DMMP saturated film shifted from 3262 to 3380 cm^{-1}. This shift indicates a disruption of the hydrogen bonding network of the TPP film. Moreover, the presence of a methoxy and phosphoryl oxygen shift confirmed DMMP was present in the film. The symmetric and asymmetric stretching of the methoxy groups from 2859 to 2856 cm^{-1} and from 2963 to 2958 cm^{-1}, respectively, implied a weak interaction between the TPP and the methoxy groups. Low wave number IR data showed the strongest interaction between the phosphoryl oxygen and the TPP film, as evidenced by a stretch from

1275 to 1234 cm^{-1}. Consequently, the phosphoryl oxygen was found to be primarily responsible for DMMP adsorption into the TPP film, with a weaker interaction between the film and the methoxy groups. The proposed bonding scheme is shown in Figure 1.16. DMMP adsorption increased linearly with TPP film thickness and the resulting DMMP saturated films were stable after several weeks. Upon heating the saturated films to 154 °C, RAIRS revealed the DMMP had been driven off and the TPP film returned to its original structure.
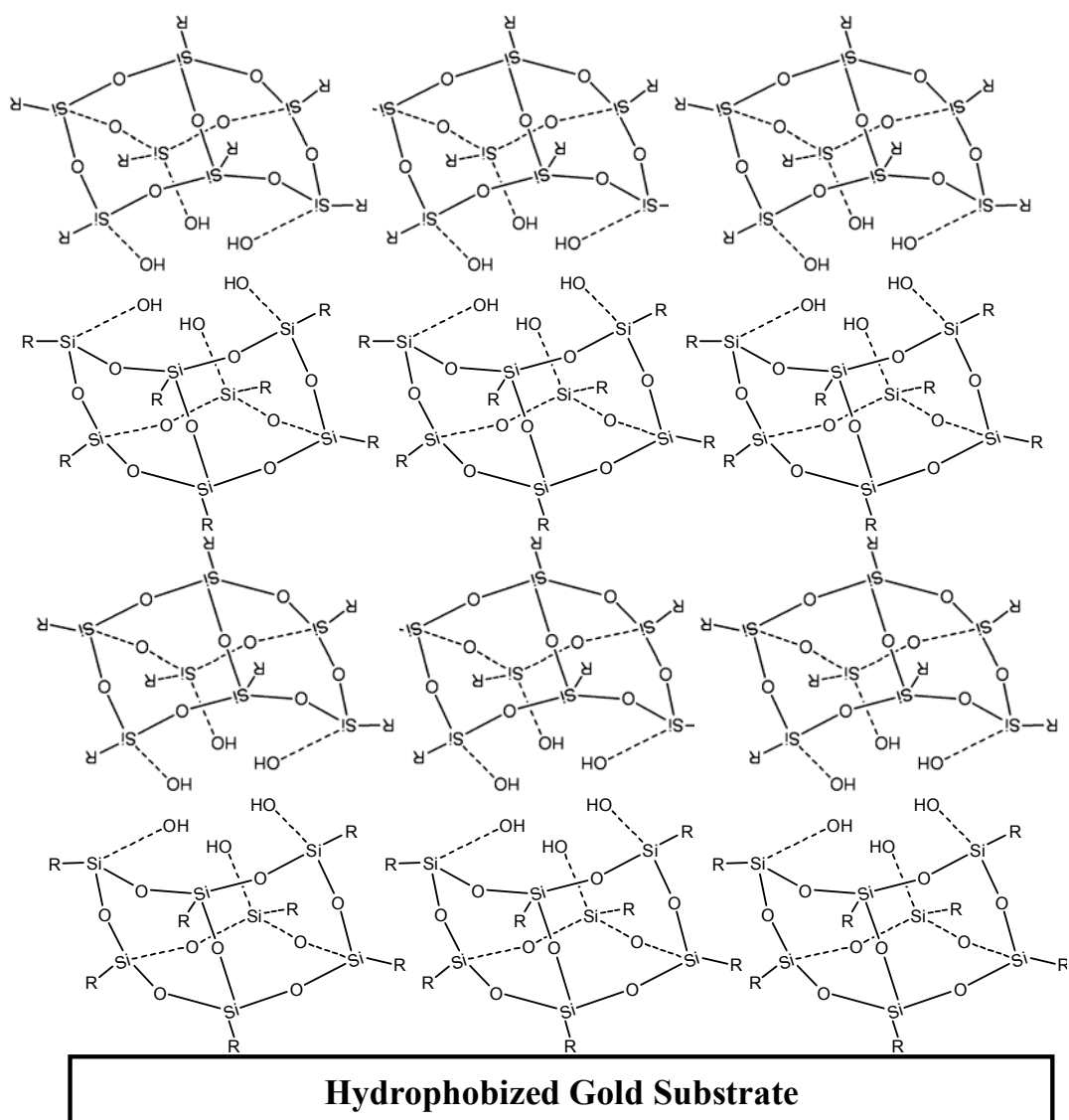
Figure 1.15 Langmuir-Blodgett films of trisilanolphenyl-POSS on gold.

TPD experiments were also conducted on the saturated DMMP-TPP films. The films were placed into a UHV chamber equipped with a mass spectrometer and subjected to a 0.1 K s^{-1} linear heating ramp. As no reaction products were observed, the major fragment of DMMP ($m/z = 94$) was used to determine the desorption energy of DMMP. This fragment created a single peak at a 154 °C, suggesting the DMMP interaction within the TPP is consistent throughout the film. The DMMP exhibited zero-order desorption kinetics and a desorption energy of 122 ± 1.0 kJ mol^{-1}. The relatively large desorption energy was attributed to hydrogen bonding between the silanols of the TPP film and the phosphoryl oxygen of DMMP.
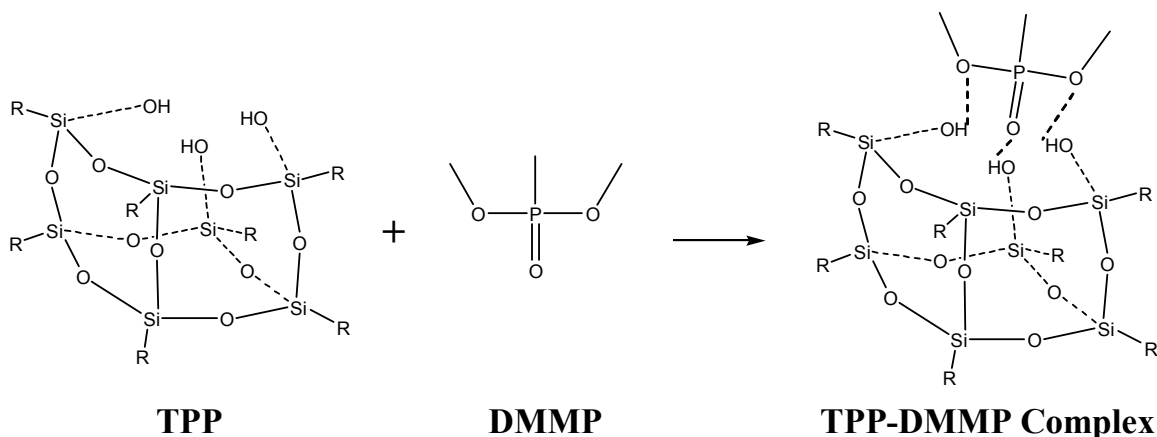
Figure 1.16 DMMP sorption onto TPP, where R is a phenyl group.[1]

1.4 Summary and Research Focus

Understanding the reaction chemistry of CWAs is important for developing improved CWA sensors, determining decomposition pathways, and producing protective coatings. Limited studies on the reactions of CWAs in solution and over metal oxides have shown that CWAs undergo hydrolysis reactions in solution to form phosphonic acids and over metal oxides to form surface bound phosphonate products. However, the

inherent danger of working with CWAs has led to the development and study of CWA simulants.

The thermocatalytic adsorption and decomposition of DMMP, the most commonly studied CWA simulant, has been examined over a variety of metal oxides. Generally, the phosphoryl oxygen bound to Lewis acid sites on the metal oxide surface at lower temperatures. As the temperature was increased, the methoxy groups decomposed, typically releasing methanol, and an irreversibly bridged or tridentate phosphate species formed on the surface. In contrast to the metal oxides, DMMP only underwent physisorption on SiO_2.

The interaction between DMMP and model organic and organic hybrid thin films has also been studied. Like SiO_2, DMMP only exhibited physisorption on these surfaces. DMMP weakly adsorbed to methyl-terminated SAMs via van der Waals interactions, and bound strongly to hydroxyl- and carboxylic acid-terminated SAMs through hydrogen bonding. DMMP also adsorbed onto and penetrated into TPP LB-films in a saturated environment, primarily through hydrogen bonding between the phosphoryl oxygen of DMMP and silanol sites of TPP. The adsorption increased with the number of film layers, and DMMP saturated films remained stable for several weeks. The DMMP was driven from the TPP film upon heating, restoring the film to its original structure.

Only a few studies have examined the effect of water on the adsorption and decomposition of DMMP. Co-adsorbed water increased the adsorption and decomposition of DMMP over MgO surfaces; furthermore, the activity of the MgO was partially restored with water pulses. Copious amounts of water resulted in some hydrolysis of DMMP over SiO_2. However, no increase in DMMP adsorption onto SiO_2

27

was observed.   Finally, water increased the adsorption of DMMP onto hydroxyl-terminated SAMs because of the formation of an extensive hydrogen bonding network, while water decreased the adsorption of DMMP onto carboxylic acid-terminated SAMs because the acid strongly bound water to the surface, reducing the available bonding sites for DMMP.

While a significant body of work exists concerning the reactions of CWA simulants over a variety of surfaces, few of these studies have quantitatively examined the sorption and desorption of CWA simulants. Consequently, my research focuses on using a quartz crystal microbalance to quantitatively determine:

1) The amount of DMMP sorbed into LB-films of TPP

2) The desorption of DMMP from LB-films of TPP

Chapter 2
Experimental Methods

2.1 Quartz Crystal Microbalance

2.1.1 Theory

A quartz crystal microbalance (QCM) crystal is composed of a thin, circular disk of quartz plated with a metal electrode typically composed of gold or platinum. The crystal is placed in an oscillator circuit and driven to its resonant frequency, which is displayed with the aid of a frequency counter. The piezoelectricity, or the generation of electricity caused by the application of a mechanical stress, of quartz is the basis of the QCM.[44-49] The change of electrical potential occurs because of the noncentrosymmetric space groups of quartz. Lacking a center of symmetry, a polar axis forms based on the dipole orientation of the atoms in the crystal lattice. Applied stresses lead to the displacement of the atoms and subsequent shifting of the dipoles, causing a change in the net charge at the crystal face. The reverse is also true – by applying a potential across the electrodes connected to the quartz crystal surface, a shear force is generated, as depicted in Figure 2.1.

A   **B**
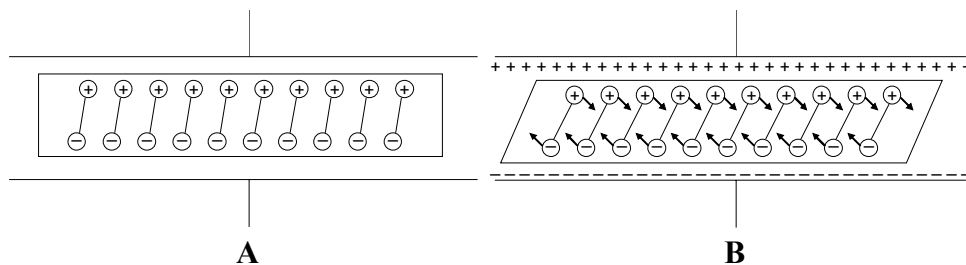
Figure 2.1 Representation of the shear force generated by the application of current to a piezoelectric material. A) The initial state of the polar, noncentrosymmetric material. B) Shear deformation caused by the reorientation of the dipoles in the electric field. The direction and magnitude of the shear is dependent on the applied potential.[44]

For AT-cut quartz crystals, which are cut from rods of quartz at a 35° angle from the x-axis, application of an alternating potential across the electrode generates a vibrational wave with an amplitude parallel to the crystal surface. The vibrational crystal motion in turn yields a transverse acoustic wave traveling at the speed of sound in quartz that moves through the thickness of the crystal, reflecting back into the crystal at the surfaces, as shown in Figure 2.2. A standing wave is created when the wavelength caused by the oscillating crystal is two times the crystal thickness. Under conditions in which a standing wave is generated, the crystal is oscillating at its resonant frequency. An applied stress, such as a change in mass or medium contacting the crystal surface, leads to a change in the resonant frequency of the oscillating crystal. Consequently, the QCM is a sensitive mass balance capable detecting nanogram or better changes in mass.[44-48]
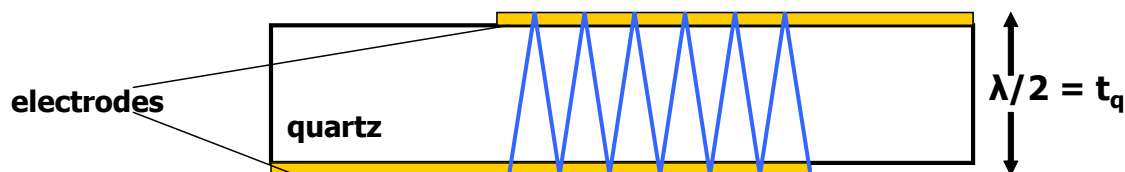
Figure 2.2 Schematic representation of the transverse shear wave generated in an AT-cut quartz crystal under the application of an alternating potential.[44]

The pioneering work with a quartz crystal microbalance was conducted by Sauerbrey, who studied the adsorption of rigid thin films to the surface of the quartz electrode in the gas phase. He discovered that the change in mass on the surface of the quartz is proportional to the change in the resonant frequency of the oscillating crystal.[50] An unloaded crystal oscillating at its resonant frequency is defined by the velocity of the

transverse sound wave and the thickness of the quartz. The sound wave velocity is in turn a function of the shear modulus and density of the quartz:

$$f_0 = \frac{v_{tr}}{2t_q} = \frac{\sqrt{\mu_q / \rho_q}}{2t_q} \tag{2.1}$$

where f_0 is the resonant frequency, v_{tr} is the sound wave velocity in quartz, t_q is the thickness of the quartz crystal, μ_q is the shear modulus of the quartz, and ρ_q is the density of the quartz.
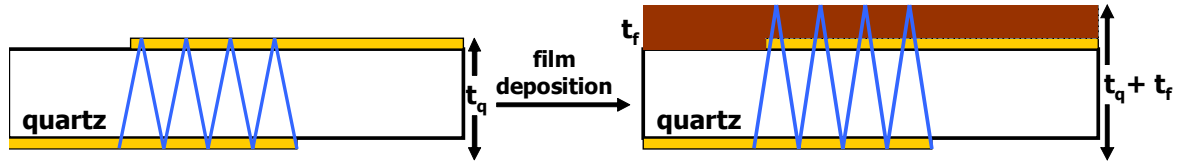
Figure 2.3 Representation of the increase in amplitude of the acoustic wave traveling through the oscillating quartz crystal caused by the addition of a thin film to the crystal surface.

When a thin film of some mass is deposited onto the crystal surface, the sound wave now travels into the film, as shown in Figure 2.3. The thin film can be treated as an incremental increase in the thickness of the quartz by making three assumptions: (1) the density and shear modulus of the thin film is the same as that of quartz; (2) there is no slip between the crystal surface and the film (i.e. the film is rigidly attached to the surface); (3) the frequency shift resulting from the mass increase is independent of radial distance. The first two assumptions are valid for thin films adsorbed from the gas phase; the effect of the third assumption is minimized by applying a uniform film and using a small active area for mass measurements.[44,48,50] By treating the thin film as an increase in

31

the thickness of the quartz and recognizing that the thickness is related to the mass change of the film divided by the product of the active area of the measurement and the density of the film, the well-known Sauerbrey equation relating the change in frequency to the change in mass is easily derived from:

$$\Delta f / f_0 = -\Delta t / t_q = -2 f_0 \Delta t / v_{tr} \qquad (2.2)$$

to yield:

$$\Delta f = -2 f_0^2 \Delta m / A \sqrt{\mu_q \rho_q} = -C_f \Delta m \qquad (2.3)$$

In Equations 2.2 and 2.3, Δf is the change in frequency, Δt is the change in thickness, A is the active area and Δm is the change in mass per area. Thus, a decrease in the observed frequency is the product of a constant (C_f) and the change in mass per unit area.
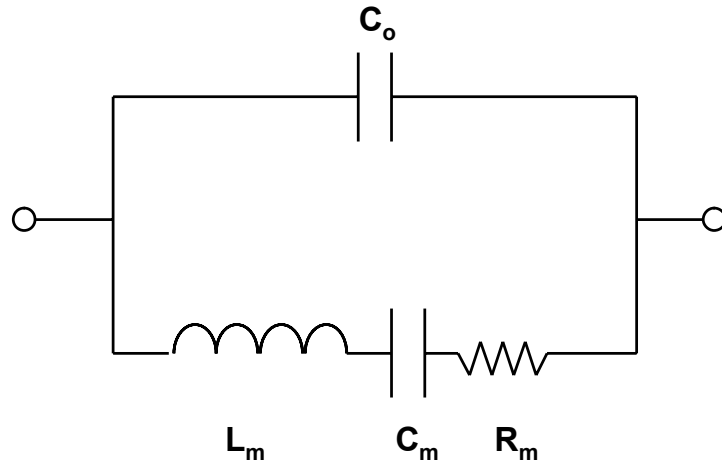
Figure 2.4 **Butterworth-van Dyke electrical model for a quartz crystal oscillating near series resonance. The inductor (L$_m$) and capacitor (C$_m$) are analogous to the inertial and elastic energy of an oscillating crystal, while the resistor (R$_m$) corresponds to frictional losses. The parasitic capacitance (C$_o$) arises from the crystal holder and mounting structures and does not depend on the piezoelectricity of the crystal.**

The behavior of a crystal oscillating near series resonance is often represented using the Butterworth-van Dyke electrical model, as shown in Figure 2.4. If an ideal quartz crystal (i.e. no resistor/frictional losses) is subjected to a AC voltage and the current is then removed, the stored inertial and elastic energies of the crystal would lead to continuous oscillation. Likewise, in an ideal circuit, energy oscillates between the inductor, which stores energy in the form of a magnetic field, and the capacitor, which stores energy in the form of electrical potential. The inertial energy of the quartz crystal relates to the inductor (L_m) and the elastic energy relates to the capacitor (C_m). Maximum surface displacement of the crystal corresponds to a fully charged capacitor in which the potential energy is at a maximum. Zero surface displacement of the crystal corresponds to a maximum field around the inductor and maximum current, i.e. the point of maximum kinetic energy. However, the quartz crystal is not ideal – there are frictional losses, which may be likened to a resistor. The motional resistance (R_m) therefore increases with viscosity of the surrounding medium. Together, the inductor, capacitor, and resistor are placed in series because they are directly affected by the piezoelectricity of the quartz. Parasitic capacitance, C_o, is also present in parallel and arises from the crystal holder, mounting structures, cables etc. Placing the crystal in an oscillator circuit allows easy determination of the resistance through impedance analysis. The QCM crystal can be driven by an automatic gain control amplifier, in which the voltage is supplied in such a way that the circuit oscillates at a frequency for which the phase shift around the loop is 0°. By nulling C_o and recognizing that the reactance of the capacitor and inductor cancel at series resonance, the supplied current must equal R_m. As the resistance is a function of the frictional losses of the medium contacting the crystal surface, it is useful for detecting

phase changes, the creation of networks, and relative viscoelastic properties of the film bound to the crystal surface.[44, 47, 48]

Strictly speaking, the Sauerbrey equation is only applicable to gas phase measurements of rigid, thin films of mass less than 2% of the crystal. At higher mass loadings, the assumptions that the film has the same density and shear modulus as the quartz are no longer valid. This situation is corrected by considering the elasticity of the film. As shown in Figure 2.5, the equivalent electrical circuit is expanded to include the inductance contributed by the mass of the film.
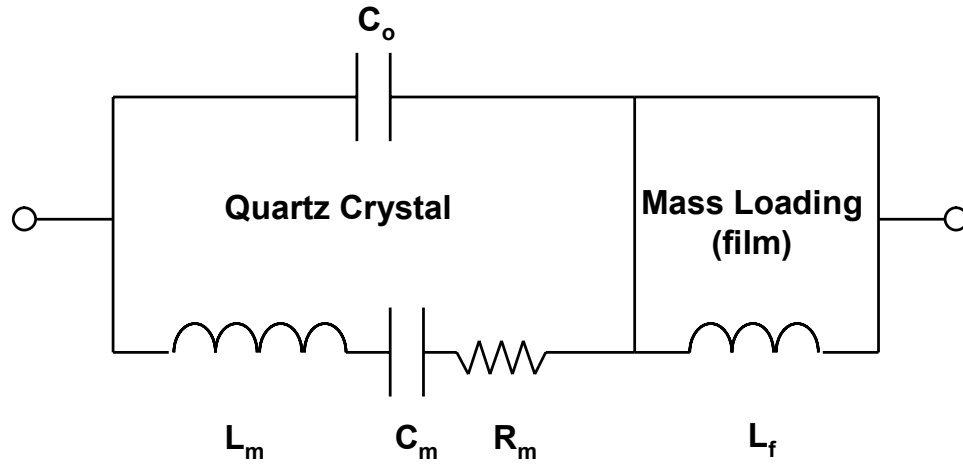
Figure 2.5 Butterworth-van Dyke electrical model for a loaded quartz crystal oscillating near series resonance. For mass loadings above 2% of the unloaded crystal, an additional inductor (L_f) is required to account for the elastic properties of the film.

Lewis and Lu[51] developed an equation that modeled the behavior of thick films in the gas phase:

$$\Delta m = \left(\frac{N_q \rho_q}{\pi Z f_L} \right) \tan^{-1} \left[Z \tan \left(\frac{\pi (f_0 - f_L)}{f_0} \right) \right] \tag{2.4}$$

$$Z = \sqrt{\frac{\rho_q \mu_q}{\rho_L \mu_L}} \tag{2.5}$$

In Equations 2.4 and 2.5, the variables are: N_q the frequency constant for an AT-cut crystal, f_0 the unloaded frequency of oscillation, f_L the loaded frequency of oscillation, ρ the density, and μ the shear modulus. The accuracy of this model depends heavily on the Z-term, or a knowledge of the film's density and shear modulus. For rigid films adsorbed from the gas phase, Equation 2.4 is valid up to 40% of the crystal's mass. However, neither the Sauerbrey equation nor the Z-match method apply to thick, viscoelastic polymer films, as the losses due to the shear motion of the film are difficult to resolve. Several groups have successfully modeled the response of thick, viscoelastic films using the QCM with dissipation (QCM-D) technique.[52-54]

Subsequent work by several groups established that QCMs could be used in liquid environments.[55-57] In liquids, the downward shift in frequency is not only caused by any mass added to the surface, but also by the viscosity and density of the liquid contacting the crystal surface. The behavior of the resonating crystal is analogous to a pendulum swinging through a fluid – the properties of the fluid affect the frequency of oscillation. The Butterworth-van Dyke equivalent electrical circuit is modified (Figure 2.6) to include an inductor, related to the liquid's density, and a resistor, related to the liquid's viscosity. Kanazawa and Gordon modeled this effect and developed an equation to predict the change in frequency contributed by the fluid, in which the density (ρ) and viscosity (η) of the fluid are considered:

$$\Delta f = -f_0^{3/2}\left(\frac{\rho_L \eta_L}{\pi \rho_q \mu_q}\right)^{1/2} \tag{2.6}$$
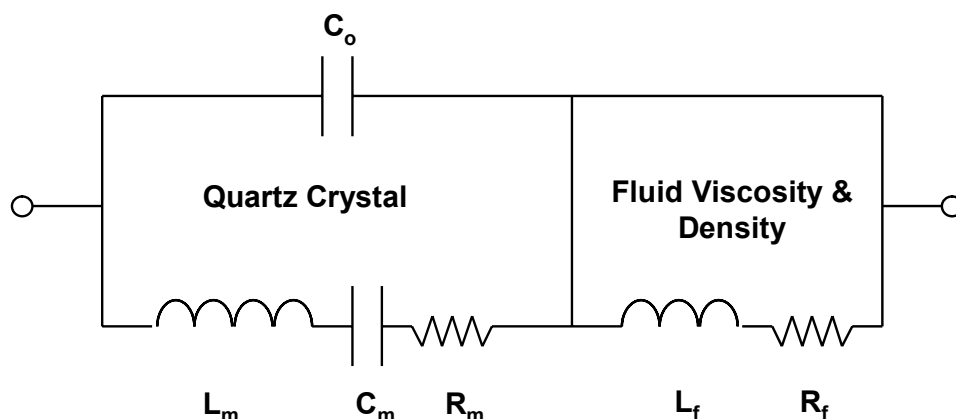
Figure 2.6 Butterworth-van Dyke electrical model for a quartz crystal oscillating near series resonance in a liquid. The density and viscosity of the fluid are accounted for by the addition of an inductor and resistor, respectively.

2.1.2 Factors Affecting QCM Measurements

Because of the sensitivity of the QCM to changes in the surrounding environment, care must be taken to minimize the effect of peripheral factors that are capable of causing frequency shifts. The interfacial slippage and non-uniform mass distribution of the film, surface roughness of the crystal, and pressure and temperature of the surrounding environment can lead to undesirable frequency shifts.[44, 58-62]

Interfacial slippage affects the accuracy of the measurements, as commonly used models rely on the "no-slip" condition: the first layer of the adsorbate at the QCM metal electrode surface is tightly bound and does not slip during the shear motion of the crystal. However, the literature suggests that interfacial slippage causes frictional losses, thereby introducing slight frequency decreases.[44]

Nonuniform mass distribution on the crystal surface causes deviations in that the crystal's shear velocity and amplitude that are radially dependent. This effect is

minimized by applying a uniform mass onto the crystal and designing a small active area of the QCM electrode.[58]

Surface roughness of the crystal affects QCM measurements because the entrapment of fluids in surface cavities will result in an additional mass component.[59, 60] The crystal surface is typically polished to minimize this effect.

Pressure can also affect the accuracy of a measurement – for example, often, one side of the crystal faces a liquid while the other is exposed to air; this places a stress on the crystal because of the hydrostatic pressure. The effect of pressure on the QCM is not well understood, but fortunately in most experiments it is likely negligible because the pressure is typically constant over the course of an experiment.[44, 61]

Temperature, while it does not significantly affect the properties of the crystal,[62] can have a dramatic affect on the properties of the surrounding medium, such as the density and viscosity of a fluid. Consequently, the temperature must remain constant during the course of an experiment.

2.1.3 Applications

The rapid development of commercially available QCMs over the last 20 years has led to a significant increase in their use for investigating physical and chemical processes through the observation of mass changes.[48] Originally designed to detect mass changes caused by gas-phase depositions, the QCM is still widely employed as a sensitive gas-phase balance.[46, 66, 64] However, the QCM is no longer limited to gas-phase detection. Several groups investigated the operation of QCMs in liquids,[55, 56] opening the door to a variety of applications, including the study of electrodeposition of metals,[57,65] electrochemical dissolution,[60,66] adsorption/desorption of surfactants,[67] changes in

conductive polymer films during redox processes,[68,69] and the study of liquid properties.[70,71] A growing area of interest involves modifying the surface of the QCM crystal electrode with a self-assembled monolayer (SAM), or some other thin film, thereby building specificity towards a particular reagent and, in effect, creating a chemical or biological sensor. QCMs have been successfully modified for use as immunosensors for proteins and antibodies,[72,73] as well as for use as specific gas-phase detectors.[74] Because QCMs are extremely sensitive to changes in surface mass, capable of rapid data acquisition in a variety of mediums with or without modification of the crystal electrode, and are relatively inexpensive and easy to operate, the range of applications and regular use of the QCM will continue to grow.

2.1.4 Instrumentation

AT-cut quartz crystals with a fundamental frequency of 5 MHz and the QCM 200 were obtained from Stanford Research Systems (Sunnyvale, CA). The crystals have a one inch diameter and are platted with gold electrodes on both sides, as shown in Figure 2.7.
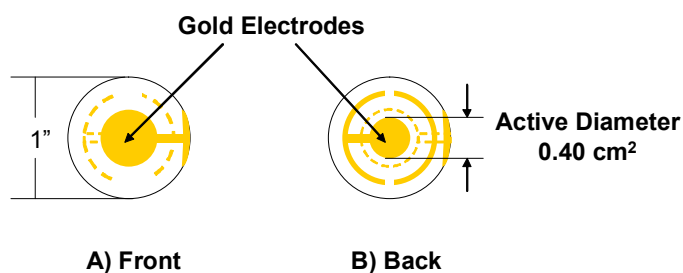
Figure 2.7 **Representation of the quartz crystals used. Both sides of the crystal are coated with gold electrodes. A) The front faces the medium of interest. B) The back creates a seal with the crystal holder and is exposed to air.**

The crystals are mounted into a Kynar® crystal holder; the front faces the medium of interest, while the back faces air and creates a seal to protect the crystal holder

interior from solutions. A BNC connector attaches the crystal holder to the QCM 25 crystal oscillator. A RJ-45 connection ties the QCM 25 oscillator to the QCM 200 frequency counter, which in turn uses a standard RS-232 port to connect to a computer. A typical experimental setup is shown in Figure 2.8. The crystal holder is suspended into a 100 mL beaker of the solution of interest. The beaker is contained in a VWR Signature Heated/Refrigerated Circulator (Model 1166D, Batavia, IL) filled with distilled water, which provided temperature stabilization to within ±0.01 °C.
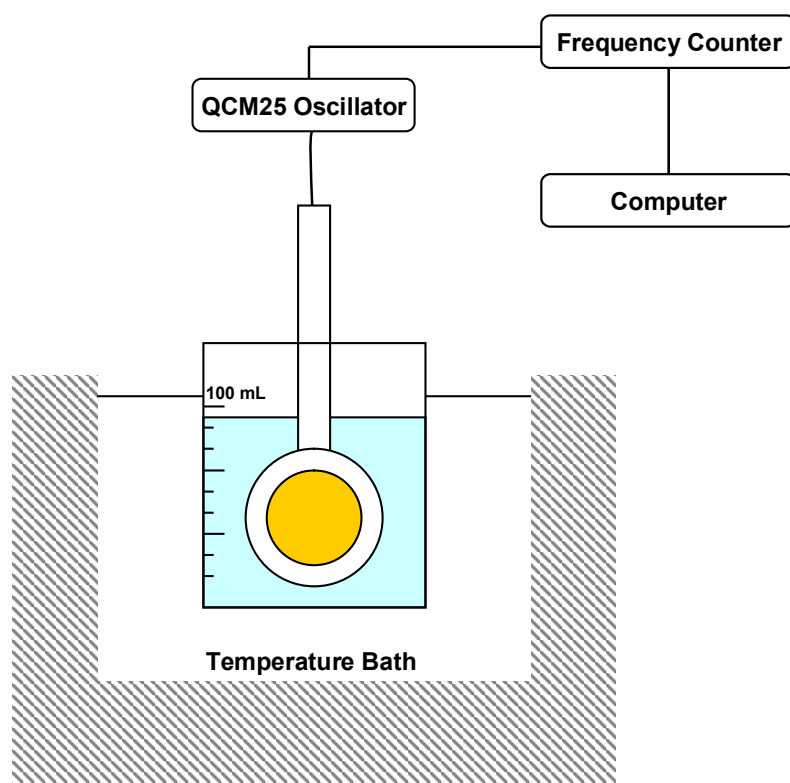
Figure 2.8 Representation of a typical QCM experimental setup. The crystal is immersed in a beaker of the solution of interest, which is held at constant temperature with the aid of a temperature bath. The oscillator provides data to the frequency counter, which in turn displays the information on a computer.

2.2 Cleaning Procedures

2.2.1 QCM Crystals

The following procedure was used to ensure a clean surface for QCM studies:

1) The crystals were kept in the original packaging provided by the supplier until use.

2) Upon removal, a crystal was placed in a 50 mL solution of 3:1 H_2SO_4 and H_2O_2 (Piranha solution) for 10 minutes to remove organic residues. *Note: Piranha solutions are extremely reactive and may result in explosions or skin burns if not properly handled; glassware containing Piranha will be hot.*

3) The crystal was then washed with copious amounts of de-ionized water and blown dry with a gentle stream of N_2 gas.

4) The crystal was then placed under a UV/ozone lamp for 10 minutes, as UV/ozone is an effective means to remove organics from the crystal surface.[75]

5) Following another rinse with de-ionized water and drying with N_2 gas, the crystal was immediately mounted into the crystal holder for use.

2.2.2 QCM Crystal Holder

The crystal holder was cleaned before each QCM experiment. Before cleaning the crystal holder, Parafilm was used to seal the crystal cavity to prevent liquid from entering and possibly flowing under the contact pins and into the electronics of the holder. Care must also be taken to prevent liquid from entering the BNC connection port. The crystal holder was then cleaned by first rinsing the holder with de-ionized water. This rinse was followed by cleaning with a de-ionized water and detergent solution. The holder was then rinsed lightly with ethanol, followed by de-ionized water, and blown dry with N_2 gas.

2.2.3 Glassware

All glassware used the in preparation of solutions, as containers into which the QCM probe was dipped, or as storage units for QCM crystals requiring multiple measurements were cleaned by immersion into a 5 L base bath (4:1 isopropanol to water, 300 g KOH) for at least 24 hours. The glassware was then rinsed with de-ionized water, followed by a rinse with 0.1 mM HCl and a final rinse with de-ionized water. The glassware was then covered and left to dry at ambient conditions.

2.3 Validation of the Experimental Technique: Self-Assembled Monolayer Formation onto Gold

2.3.1 Introduction

Self-assembled monolayers (SAMs) are unidirectional monolayers that spontaneously form onto solid substrates immersed into a solution of active surfactant in an organic solvent.[76] A number of SAM systems are known to form, including alkyl silane molecules on silicon oxide and alkyl carboxylates on aluminum, though alkanethiol self-assembly onto gold [111] is the most studied.[77] Alkanethiols are popular because of their potential use as sensors or surface modifiers, in which surface properties can be modified by using thiols with different functional endgroups.[78] The system studied here is the adsorption of 1-dodecanethiol onto the gold electrode of a QCM crystal (Figure 2.9). A further review of alkanethiol SAMs may be found in the literature.[76-80]
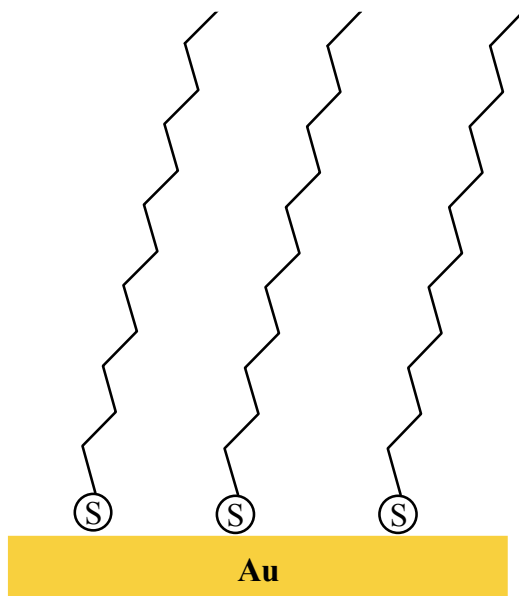
Figure 2.9 **Formation of 1-dodecanethiol onto gold. The initial adsorption takes less than one minute, though ordering of all the alkyl chains takes several hours.**[78]

2.3.2 Experimental Procedure

1) A quartz crystal was cleaned in accord with Chapter 2.2.1.

2) The stable frequency (<1 Hz fluctuation) of the clean crystal at 23 °C was recorded in a beaker of air immersed in a water bath (Figure 2.8).

3) The crystal, still in its holder, was removed from the setup and placed in a 1 mM solution of 1-dodecanethiol in ethanol for 12 hours.

4) The SAM-coated crystal was dried with a gentle stream of N_2 gas.

5) The stable frequency of the SAM-coated crystal at 23 °C was recorded in a beaker of air immersed in a water bath (Figure 2.8).

2.3.3 Results and Discussion

The frequency difference between the clean and SAM-loaded crystal is attributed to the adsorbed mass of 1-dodecanethiol onto the QCM surface. The theoretical frequency shift is readily calculated via the Sauerbrey equation (Equation 2.3) to be 8.8 Hz, assuming the packing area per thiol molecule is 21.6 $Å^2$ and the active measurement area for QCM200 crystals is 0.40 cm^2.[77] A 1 Hz change corresponds to 17.7 ng/cm^2.[50] Thus, the Sauerbrey equation predicts a frequency shift equal to the adsorption of 155.8 ng of 1-dodecanthiol per cm^2. The frequency difference between the clean and SAM-loaded crystal was experimentally measured in triplicate to be 10.5 ± 0.5 Hz. The frequency shift is readily converted to mass per unit area using the Sauerbrey equation and found is 185.9 ± 8.9 ng/cm^2. These results are plotted in Figure 2.10.
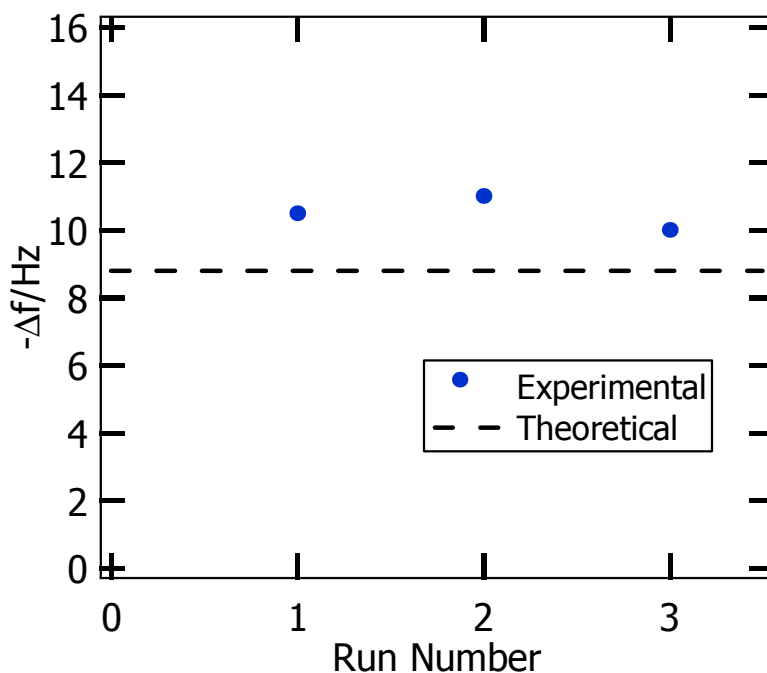
Figure 2.10 Frequency shift caused by the adsorption of a 1-dodecanethiol SAM on the gold electrodes of a QCM crystal.

The experimentally determined shift was reproducible; further, the experimental and theoretical shifts agree within 15%. The difference likely stems from the assumption of a perfectly smooth gold [111] surface in calculating the theoretical shift. The actual surface of the QCM crystal electrodes has an average surface roughness of 50 Å, thereby increasing the area available for alkanethiol adsorption.[81]

Chapter 3
Polyhedral Oligomeric Silsesquioxane Langmuir-Blodgett Films: Sorption of Dimethyl Methylphosphonate

3.1 Introduction

3.1.1 Langmuir-Blodgett Films

A Langmuir-Blodgett (LB) film is a well-ordered, multilayer film created by the repeated transfer of Langmuir monolayers onto a solid substrate. Langmuir monolayers are composed of amphiphilic species at the air/water interface: the hydrophobic group prevents dissolution into the aqueous subphase, while the hydrophilic group binds the species to the water surface.[82] Langmuir monolayers have been formed from a wide variety of amphiphiles, including alcohols,[83] esters,[84] aromatic compounds,[85] polymers,[86] and phospholipids.[87] Thin films formed by the LB-method afford precise control over film thickness, homogeneous film deposition over large areas, and the ability to vary the multilayer composition. Such well-ordered, tailored films may find use in sensors, detectors, displays, and electronic circuit components.[82]

Benjamin Franklin first records the formation of a monolayer film in 1774, though he failed to grasp the full significance of his observation. He observed that a teaspoon of oil formed a smooth layer over a half acre of a pond.[88] Nearly one hundred years later, Lord Rayleigh's studies of oil/water systems led to his conclusion that the oil layer formed a monolayer, the thickness of which could be estimated via the area of spreading.[89] In the late 1890s, Agnes Pockels developed a crude surface balance in her kitchen sink – the basis for the Langmuir trough – and published the first pressure-area isotherm.[90] In the early 1900s, Irving Langmuir quantitatively studied the transfer of floating fatty acid, ester and alcohol monolayers from water to solid substrates on his

Langmuir film balance. His work confirmed that the monolayer thickness is one molecule and that short-range forces are responsible for the formation of well-ordered films.[91] In 1919, Katherine Blodgett first published detailed descriptions of the creation of multilayer films through the sequential deposition of fatty acid monolayers onto a glass slide using a Langmuir trough.[92] Over the last one hundred years, Langmuir-Blodgett (LB) films have gained increasing popularity as a means to study model systems for biomembrane research and multilayer coatings. Because their thickness and order is controllable at a molecular level, LB-films are also expected to be useful in molecular electronic and bioelectric devices.[93]
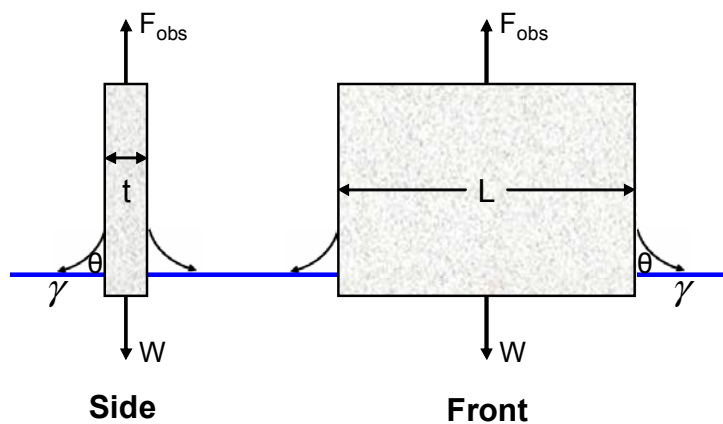
Figure 3.1 Forces acting upon a Wilhelmy plate.

A LB-trough is routinely used to create surface pressure-area isotherms.[82] This isotherm is a two-dimensional analog of a pressure-volume diagram and it provides quantitative characterization of the thermodynamic state of the monolayer at the interface.[82,94] The surface pressure, defined as the difference between the surface tension of a film covered surface (γ) and the pure liquid subphase (γ_0), is determined via the Wilhelmy plate technique. This method involves determining the forces experienced by a thin plate of paper or platinum partially immersed into the subphase. The plate is

suspended beneath a balance and, assuming the buoyant force is negligible, the observed force recorded by the balance is the sum of the gravitational force of the plate and the surface tension acting along the perimeter of the plate (Figure 3.1). Consequently, if the weight and perimeter of the plate are known, as is the wetting of the plate in the subphase, the surface tension and surface pressure are readily calculated by Equation 3.1 and 3.2, respectively.

$$\gamma = \frac{F_{obs,film} - W}{2(L+t)\cos\theta} \qquad (3.1)$$

$$\Pi = \gamma_O - \gamma = \frac{F_{obs,O} - F_{obs,film}}{2(L+t)\cos\theta} \qquad (3.2)$$

In Equations 3.1 and 3.2, F_{obs} is the force measured by the Wilhelmy plate, W is the gravitational force, L is the length of the plate, t is the thickness of the plate (usually negligible), and θ is the contact angle between the plate and the subphase ($\theta = 0°$ for complete wetting). By measuring the surface pressure as a function of the surface area available to each molecule of a monolayer, a surface pressure-area (Π-A) isotherm can be created.
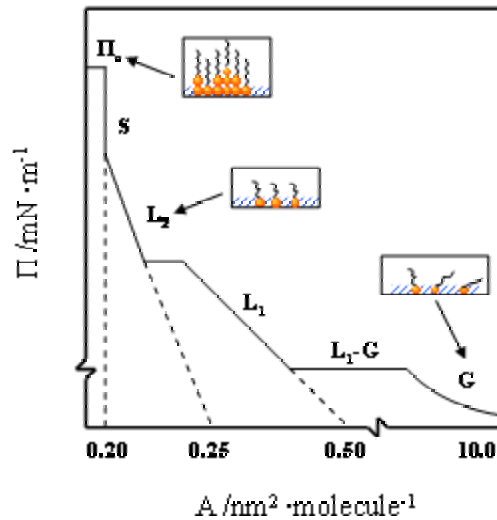
Figure 3.2 Generalized Π-A isotherm.

A generalized Π-A isotherm for a fatty acid is shown in Figure 3.2. Just as in three dimensions, the monolayer exhibits different phases. The phases and their transitions are a function of the physical and chemical properties of the amphiphile (i.e. hydrocarbon chain length and headgroup), subphase temperature, and subphase composition. At very low surface concentrations, the monolayer is in the gas (G) phase. The molecules do not interact and arrange randomly on the surface. As the surface area is decreased, the molecular surface density increases, leading to interactions between the molecules and a subsequent increase in order. Here, the liquid-expanded (LE or L_1) phase may occur, characterized by liquid-like order. For fatty acids in the L_1-phase, the hydrophilic head remains translationally disordered and the hydrophobic chains are conformationally disordered. Upon further compression, the condensed (LC or L_2) phase may be encountered. This phase is more solid-like in character and therefore less compressible than the L_1-phase. Here, the fatty acid head groups are closely packed and the hydrophobic chains are nearly normal to the water surface. The tilt angle of the hydrophobic chains with respect to the subphase can vary, leading to multiple L_2-phases.[95] Upon further compression, a solid (S) phase can form, in which the molecules arrange into a packed, ordered monolayer. Continued compression leads to the collapse surface pressure (Π_c), at which the monolayer collapses into a multilayer state.[95] Monolayer collapse may also occur via dissolution of the monolayer into the subphase above some critical surface concentration, as in the case of poly(ethylene oxide) and monolayers on water. It is important to note that not all molecules exhibit all of these phases. For example, long chain amphiphiles like arachidic acid often move straight from the gas phase to the ordered L_2-phase, skipping the L_1-phase. Similarly, short chain

amphiphiles, such as DLPC (1,2-dilauroyl-*sn*-glycero-3-phosphocholine), may only exhibit a L_1-phase without forming any L_2-phases prior to film collapse.[96]
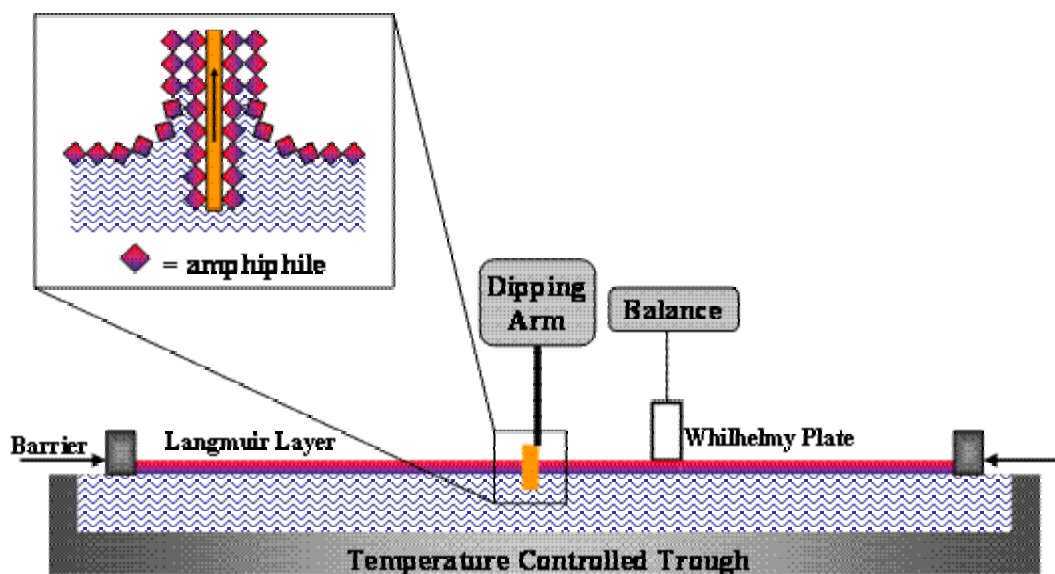
Figure 3.3 Schematic representation of a modern LB-trough.

LB-troughs are also used to create well-ordered multilayer films. A schematic of a modern LB-trough is shown in Figure 3.3. The subphase is contained in a trough, typically composed of Teflon®, and is temperature-controlled by circulating water through channels beneath the trough. The Langmuir monolayer is spread on the surface of the subphase, and a dipping arm repeatedly immerses the substrate into the trough and through the interface to transfer the desired multilayer LB-film. The barriers are computer controlled, thereby allowing the surface area per amphiphile and surface pressure (Π) of the trough to be held constant during the deposition process. The inset in Figure 3.3 depicts Y-type deposition – a hydrophobized substrate is immersed into the trough and the hydrophobic portion of the amphiphile bonds to the surface, forming the first layer on the substrate. Raising the substrate through the monolayer creates a second layer through hydrophilic interactions between the first layer on the substrate and the

Langmuir film at the air/water interface. The multilayer film is formed by repeated lowering and raising of the substrate through the monolayer. In contrast, X-type deposition adds monolayers to the substrate only as the substrate is lowered from air to water. Z-type deposition adds monolayers to the substrate only as the substrate is raised from water to air.[82, 97] It is important to note that the conformation of molecules in LB films may differ from their expected state (on the basis of the deposition type) because of molecular rearrangement.

3.1.2 Trisilanolphenyl-POSS

Silsesquioxanes refer to compounds with the empirical formula $RSiO_{1.5}$. Several silsesquioxane structures having this formula are possible, including the ladder-type and T_8 cube, as shown in Figure 3.4. (Note: In silsesquioxane chemistry, the symbols M, D, T, and Q are used to represent framework silicon atoms which possess 3, 2, 1 and 0 organyl substituents, respectively. Subscripts indicate the number of silicon atoms with the various designations.) The substituents on the silicon atoms are variable and include hydrogen, alkyl, alkenyl, alkoxy, and aryl groups. Ladenburg first reports the formation of silsesquioxane by-products in the late 1800s.[98] The first oligomeric silsesquioxanes were isolated by Scott in 1946,[99] though the breakthrough development in the controllable synthesis of silsesquioxanes did not occur until Brown and Vogt's studies in the 1960s.[100] They reported the formation of heptameric trisilanol (T_7) by the hydrolytic condensation of cyclohexytrichlorosilane in aqueous acetone (Figure 3.5) Hexameric and octameric by-products were also formed in this reaction.
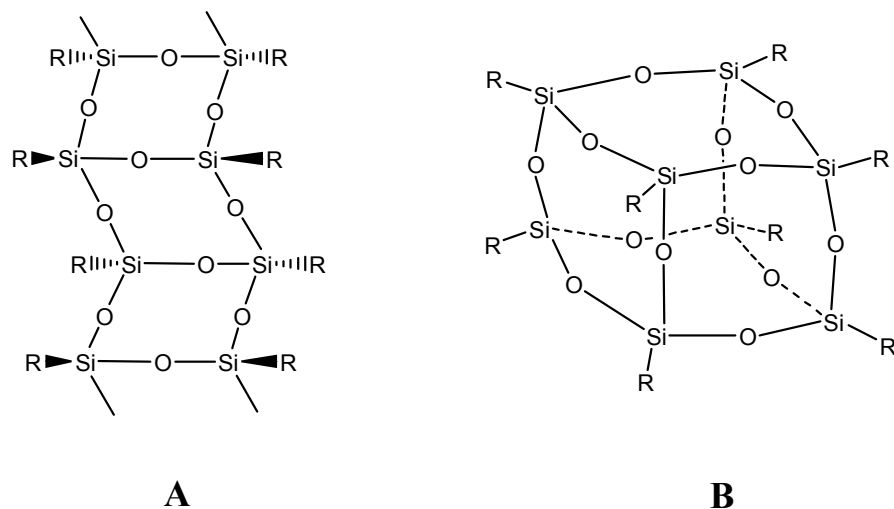
Figure 3.4 Two possible silsesquioxane structures: A) Ladder-type, B) T$_8$ cube.

Trisilanol (T$_7$) cages can undergo a variety of corner-capping reactions. T$_7$ can be substituted with transition metals to form metallosilsesquioxanes, which have shown activity as catalytic precursors for alkene polymerization.[101] T$_7$ can also be capped with organic polymerizable groups, as shown in Figure 3.5. These compounds are collectively referred to as polyhedral oligomeric silsesquioxane (POSS) monomers.[102] POSS monomers undergo polymerization to form organic-inorganic hybrid homopolymers and copolymers.[103,104] POSS hybrids offer increased thermal and oxidation stability, as well as resistance to degradation by UV-light. Recent applied research into POSS materials has focused on high-temperature and space-survivable coatings,[105] semi-conducting polymers,[106] and shape-memory materials.[107]
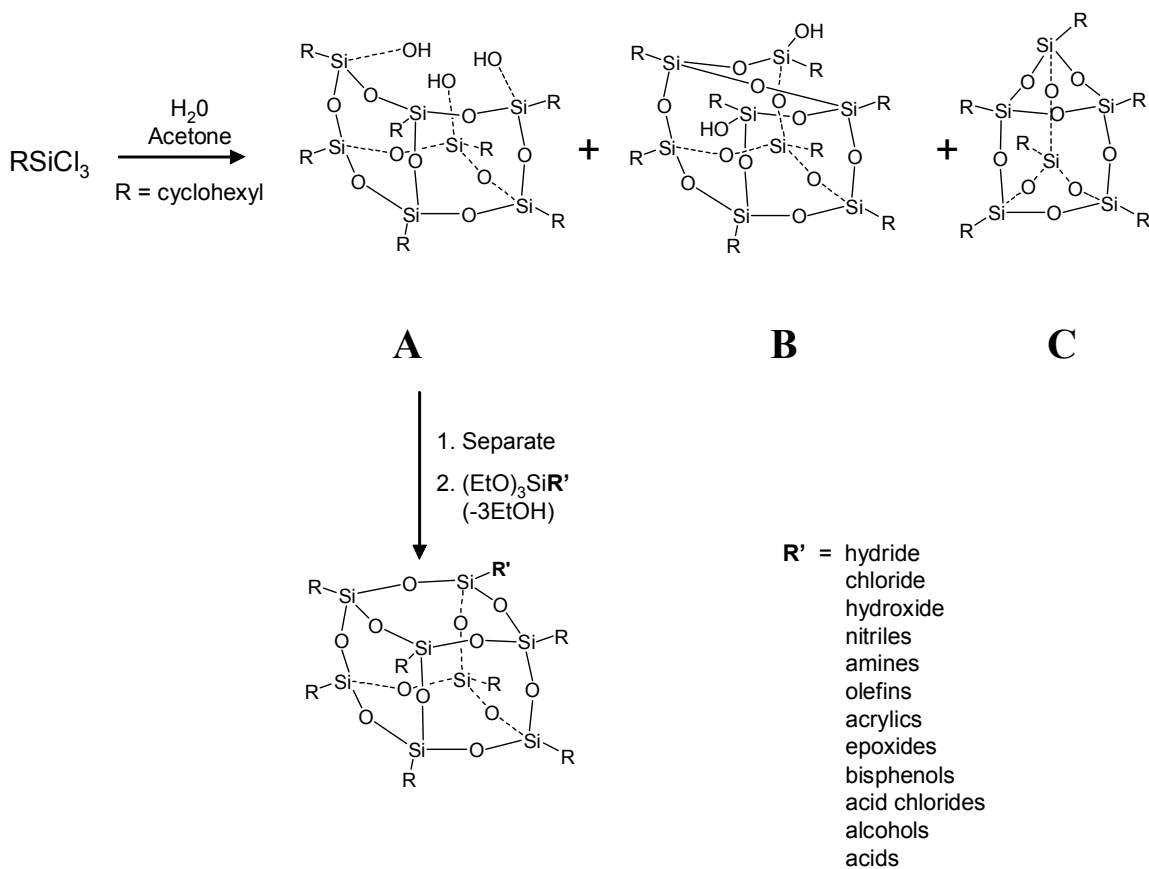
Figure 3.5 Synthesis of heptameric trisilanol (T$_7$) and POSS molecules: A) T$_7$, used to create POSS molecules, B) the octameric silanol by-product, and C) the hexameric by-product.[100]

Esker's group has spearheaded the investigation into the characteristics of thin LB-films of trisilanolphenyl-POSS (TPP). Their research has primarily focused on the dewetting and surface dynamics of poly(t-butyl acrylate) and TPP blend films,[108, 109] ion effects on TPP as an adhesion promoter,[110] and the pH effects on TPP stability.[111] As shown in Figure 3.6, TPP contains peripheral hydrophobic phenyl groups, as well as hydrophilic silanol groups. Consequently, the amphiphilic TPP will form a monolayer at the air/water interface. Π-A isotherms of TPP indicate a collapse pressure of 12 mN/m and a limiting area equal to 155 Å^2/molecule.[112] LB-films of TPP prepared below the

collapse pressure (e.g. 8-10 mN/m) are known to form well-ordered multilayer structures.[112]   Ellispometry measurements of TPP films reveal a film thickness of 0.84 nm/layer.[109]
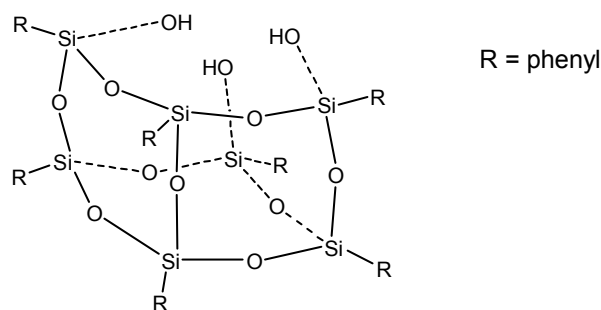
Figure 3.6 Structure of trisilanolphenyl-POSS (TPP).

3.2 Experimental Aspects

3.2.1 Materials

Ultrapure water (Millipore, Milli-Q Gradient A-10, 18.2 MΩ, < 5 ppb organic impurities) was used for cleaning the LB-trough.   1-dodecanethiol (98%) and DMMP (97%) were purchased from Aldrich.   HPLC grade dichloromethane and chloroform were purchased from EMD Chemicals Inc.   HPLC grade isopropyl alcohol was obtained from Fisher Scientific.   1,1,1,3,3,3-hexamethyldisilizane (99.9%) was obtained from Sigma-Aldrich.   TPP was obtained from Hybrid Plastics, Inc.   All chemicals were used as received.

3.2.2 Langmuir-Blodgett (LB) Film Deposition

The quartz crystal substrates were cleaned in accordance with the procedure outlined in Chapter 2.2.1.   After cleaning, the crystals were placed in a sealed glass jar containing 0.5 mL of 1,1,1,3,3,3-hexamethyldisilizane (HMDS).   The jar was placed in an oven at 80 °C for approximately 12 hours.   This procedure hydrophobized the exposed quartz surfaces of the QCM crystal.   The crystal was then placed in a 1 mM solution of 1-

dodecanethiol in ethanol for approximately 12 hours. A SAM formed on the gold electrode surface of the QCM crystal. As a result, the entire surface of the QCM crystal was hydrophobized in preparation for LB-film deposition.

The LB-films were created using a standard LB-trough (KSV 2000, KSV Instruments, Inc.) housed in a plexiglass box. Dichloromethane, followed by a rinse with ultrapure water, was used to clean the trough prior to use. Isopropyl alcohol and ultrapure water were used to clean the trough barriers. The clean trough was then filled with ultrapure water. A ~0.05 mg/mL solution of TPP in chloroform was spread onto the air/water interface to a surface pressure between 4.5-6 mN/m to avoid the formation of a multilayer.

Upon evaporation of the chloroform, the trough barriers were compressed to create a surface pressure of 8.4 mN/m. This surface pressure was held constant during the film deposition process. The hydrophobized QCM crystal was raised and lowered through the TPP monolayer at a dipping rate of 15 mm/sec, with an upper and lower delay of 3 sec. After depositing the desired number of TPP layers, the QCM crystal was immediately placed into a Petri dish and sealed with Parafilm. The crystal was stored at ambient conditions until use, upon which it was cleaned with a gentle stream of ultra-pure N_2 gas.

3.2.3 QCM Setup and Measurements

The QCM setup used for studying DMMP sorption into TPP LB-films is depicted in Figure 3.7. The crystal and crystal holder were sealed within a N_2-purged 100 mL beaker and partially immersed in a temperature bath held at 35 °C. The following list outlines the procedure taken for measuring the sorption of DMMP into LB-films of TPP:

1) A quartz crystal was cleaned in accord with Chapter 2.2.1.

2) The stable frequency of the hydrophobized crystal was recorded in the setup shown in Figure 3.7.

3) LB-films of TPP were created in accord with Chapter 3.2.2.

4) The stable frequency of the TPP-loaded crystal was recorded in the setup shown in Figure3.7.

5) ~150 µL of DMMP was injected into the 100 mL beaker through the injection port. DMMP is a liquid at room temperature; running the experiment at 35 °C raises the gas-phase concentration.[112]

6) The stable frequency after DMMP sorption was recorded in the setup shown in Figure 3.7.
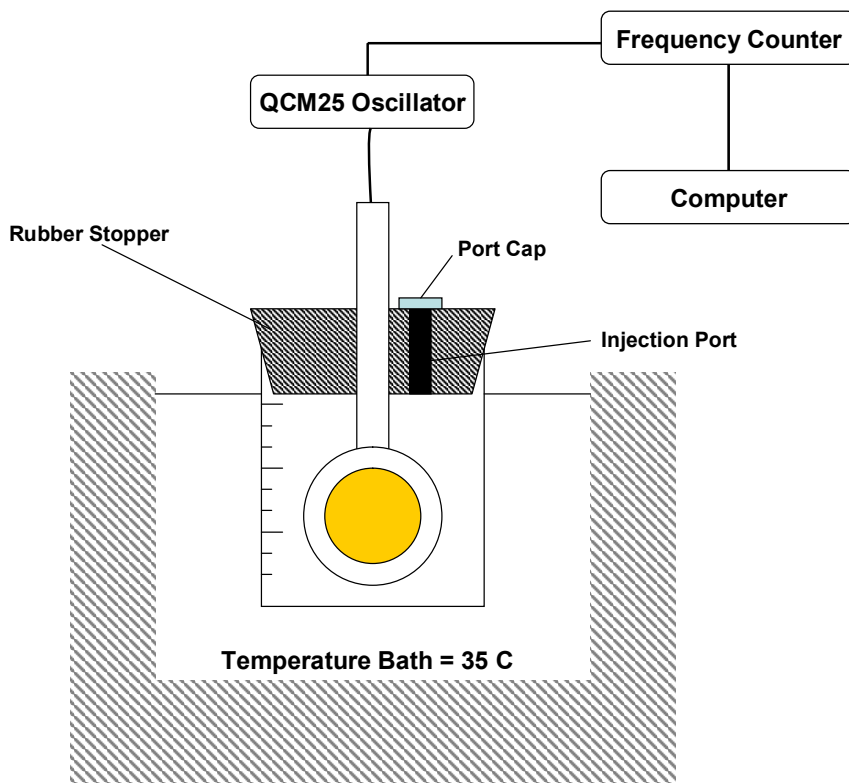
Figure 3.7 Representation of the setup used in the sorption studies of DMMP into LB-films of TPP.

3.3 TPP Film Density via the QCM

The density of the TPP films was determined using the QCM and found to be in good agreement with the literature. The frequency of the SAM/HMDS-coated quartz crystal was measured in N_2 at 35 °C and then removed from the setup. The frequency shift of the crystal after deposition of LB-films of TPP was also measured in N_2 at 35 °C, allowing the mass of TPP deposited on the active area of the crystal to be calculated according to the Sauerbrey equation.

By determining the frequency shift of the TPP-coated crystal relative to the SAM/HMDS value, the density of the TPP films is calculated as follows. The density of the TPP film (ρ_{TPP}) is the mass (Δm_{TPP}) over the volume of the film. The volume of the film is a product of the active area of the crystal ($A \sim 0.40$ cm^2), the thickness of each TPP layer ($t = 0.84$ nm),[108] and the number of TPP layers (N_{TPP}).

$$\rho_{Tpp} = \frac{\Delta m_{TPP}}{A \cdot t \cdot N_{TPP}} \tag{3.3}$$

Because the crystal was removed from the holder, a ± 2 Hz error was introduced into the measurement of the frequency shift. This error arises from the tightness of the cap exerting pressure on the crystal, affecting its resonant frequency; it was minimized by cutting a notch in the crystal holder and cap, lining up the notches before each run, and thereby reproducing the cap pressure to within ± 2 Hz. Thus, the average film density of the TPP LB-films was determined to be 1.30 ± 0.03 g/cm^3. This value is in good agreement with the ellispometry value (1.33 g/cm^3) of TPP.[109]

3.4 DMMP Sorption into TPP Films in a Saturated Environment

The LB technique was used to form TPP films of 10, 20, 30, 40, 50, and 60 layers onto the QCM crystals. The frequency shift caused by DMMP sorption into the TPP films increased linearly with the number of TPP layers (Figure 3.8), in agreement with the findings from Ferguson-McPherson *et al.*[1] The kinetics of DMMP sorption into the TPP films varied from 10 minutes to 4 hours and was not found to be a function of film thickness. Rather, the quality of a particular TPP LB-film likely determined the adsorption kinetics. A well-ordered TPP film would more effectively slow the sorption of DMMP because the hydrophobic phenyl groups would serve to block the polar DMMP molecules. If pinhole defects were present, the sorption would obviously be much faster.
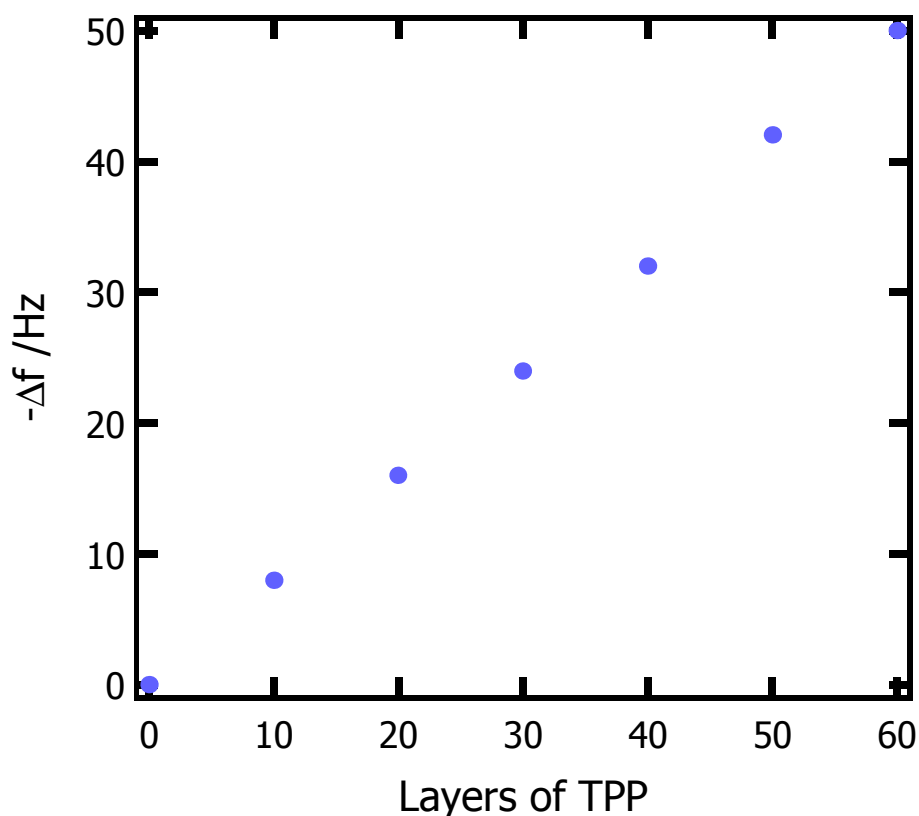
Figure 3.8 QCM frequency shift caused by the sorption of DMMP into TPP LB-films at 35 °C. The DMMP sorption increases linearly with the number of TPP layers

The Sauerbrey equation was used to convert the frequency shift to mass per unit area and subsequently to moles of DMMP sorbed into the TPP film. As shown in Figure 3.9, the DMMP binds to TPP in a 1:1 molar ratio, meaning that one DMMP molecule binds to each TPP molecule. This 1:1 molar ratio translates into 1074 μmol of DMMP sorbed per gram of TPP LB-film. The theoretical value for 1:1 sorption is readily calculated using the Sauerbrey equation, the active area of the crystal, the limiting area of a TPP molecule, and the molar mass of TPP. Combining this conclusion of 1:1 molar sorption with the RAIRS data from Ferguson-McPherson indicating hydrogen bonding between the three silanol groups of TPP and the three oxygen species of DMMP,[1] the bonding scheme shown in Figure 1.16 is proposed to occur throughout the TPP film in the presence of a saturated DMMP environment.
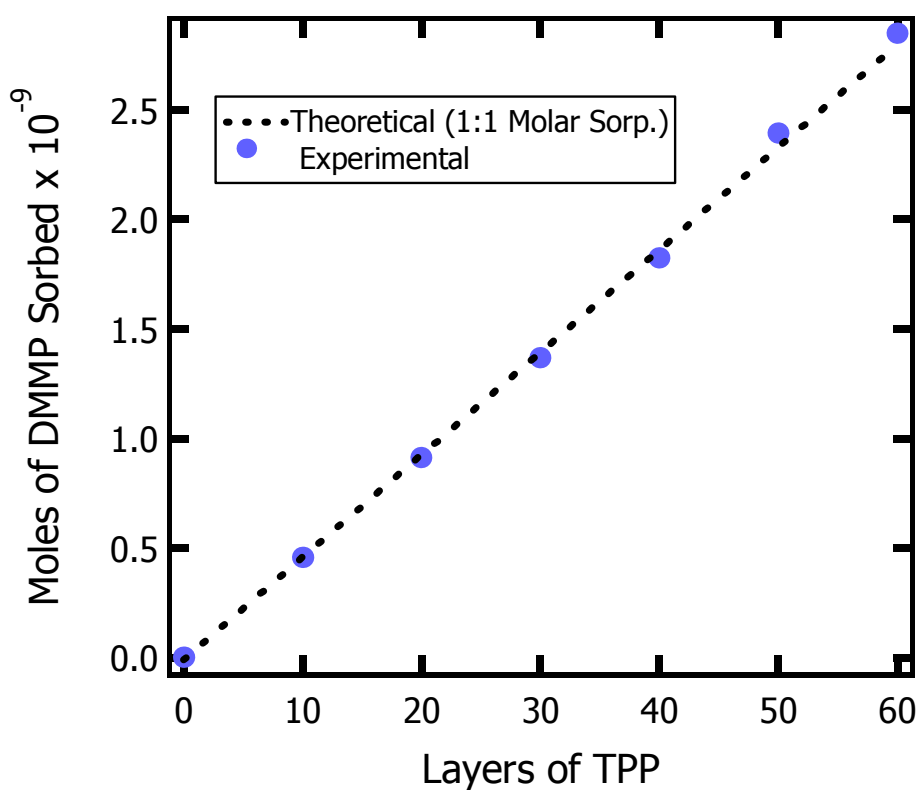
Figure 3.9 Moles of DMMP sorbed into TPP LB-films at 35 °C. The DMMP sorbs into the TPP films at a 1:1 molar ratio.

3.5 Desorption Kinetics of DMMP from Saturated LB-films of TPP

DMMP was found to desorb from the TPP LB-films under ambient conditions. The frequency of the QCM crystal for a 20-layer and a 60-layer DMMP saturated TPP film was recorded under the conditions noted in Chapter 3.2.3. Each crystal was then placed in a clean, sealed Petri dish under ambient conditions for one week. The frequency of both QCM crystals under identical conditions was again recorded. In both cases, the frequency increased after one week, indicating a loss of mass equal to nearly one-third of the DMMP. Although Ferguson-McPherson indicated that the DMMP-saturated TPP films were stable for several weeks, quantitative analysis of the RAIRS data for these films was not provided.[1]
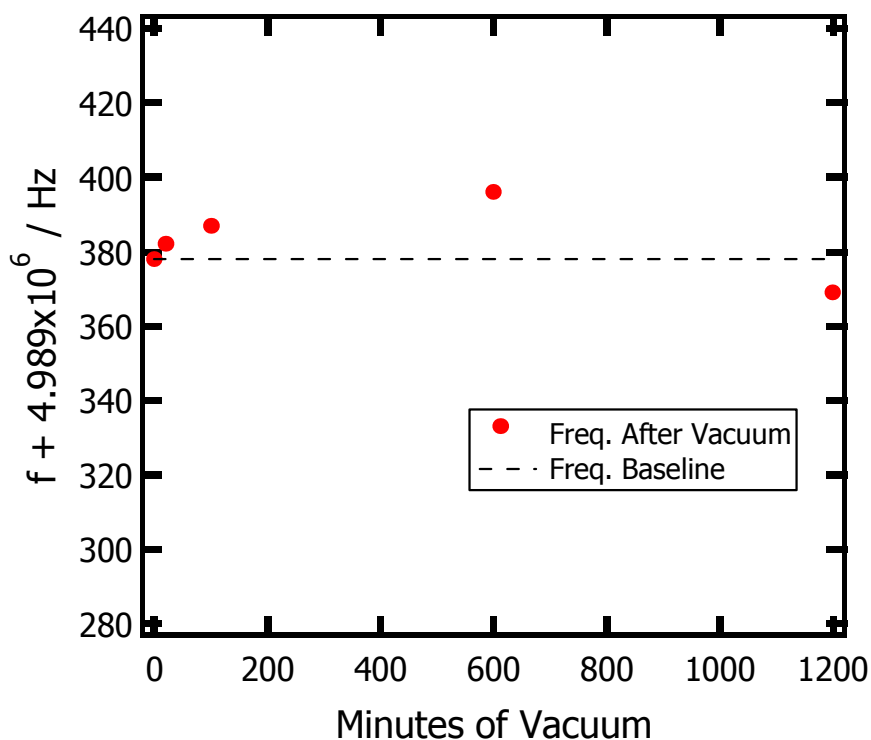
Figure 3.10 Effect of vacuum on the equilibrium frequency of a 150-layer TPP loaded QCM crystal. The frequency returns to within ± 8 Hz of its initial baseline value after turning off the vacuum.

To facilitate the study of the desorption kinetics of DMMP from TPP LB-films, the setup in Figure 3.7 was modified to pull 22 inches of vacuum on the sealed container. Pulling vacuum on the system created an unfavorable increase in frequency that masked the frequency change contributed by the desorption of DMMP, thus preventing *in situ* measurements. However, pulling vacuum on the TPP film did not significantly affect the equilibrium frequency of the crystal. As shown in Figure 3.10 for a 150-layer TPP film, the frequency of the crystal returned to its initial value (± 8 Hz) after the vacuum was turned off. Consequently, the vacuum was cycled on and off at regular intervals, and the equilibrium frequency value was recorded between each vacuum cycle.
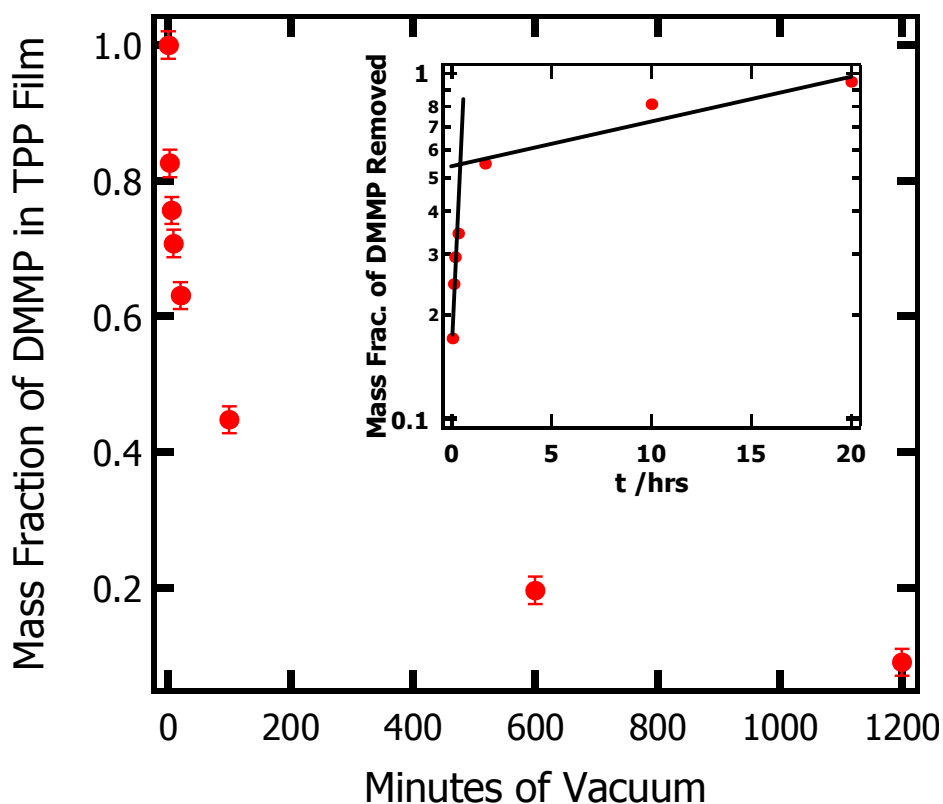
Figure 3.11 Desorption kinetics of DMMP from a 150-layer TPP LB-film at 35 °C. Two experiments were performed. The data points represent the average with one standard deviation error bars. The inset is expressed in terms of DMMP removal to clearly show the two different kinetic regimes.

A 150-layer LB-film of TPP was created and DMMP was injected into the sealed container as outlined in Chapter 3.2.3. The frequency shift associated with DMMP sorption indicated a 1:1 molar ratio of DMMP to TPP. Vacuum was then intermittently pulled on the system. All of the DMMP desorbed from the TPP film over the period of about a day. DMMP was again injected into the system and the TPP film resorbed the DMMP in a 1:1 molar ratio. This process of DMMP injection and subsequent DMMP desorption under vacuum at 35 °C was completed twice (Figure 3.11). Plotting the natural logarithm of the mass fraction versus time reveals two desorption phenomena – both exhibiting first order desorption kinetics. The rate constants for the early and late stage desorption were determined to be k = 1.59 ± 0.15 hr^{-1} and k = 0.112 ± 0.007 hr^{-1}, respectively. Assuming a typical pre-exponential factor of 10^{13} s^{-1}, the early and late time adsorption energy of DMMP within the TPP film is calculated from the Arrhenius equation to be 102 ± 6 kJ/mol and 109 ± 6 kJ/mol, respectively. The error includes the propagation of the error from the rate constant and also an order of magnitude error associated with the assumed value for the pre-exponential factor. Ferguson-McPherson *et al.* found only a single desorption energy of 122 ± 1 kJ/mol for removal of DMMP from the TPP film.[1] In contrast, the results here suggest two distinct bonding interactions between DMMP and the TPP film, both following first order desorption kinetics. When the film is saturated with DMMP in a 1:1 molar ratio, a weaker bonding interaction is observed. As DMMP is driven from the film, more silanol sites are available to interact with the DMMP, resulting in a transition to a stronger bonding environment after half of the DMMP has been desorbed from the film.

3.6 Summary

The sorption and desorption of DMMP from TPP LB-films has been quantitatively studied using a QCM. The sorption of DMMP into TPP increases linearly with the number of TPP layers, in agreement with the literature.[1] Further, DMMP binds to the TPP in a 1:1 molar ratio, resulting in the sorption of 1074 μmol of DMMP per gram of TPP LB-film. This value is actually larger than the degradation capacity of alumina-supported iron and cerium oxide surfaces, reported to be 510 μmol of DMMP per gram of metal oxide at 25 °C.[19] The DMMP desorbs from the TPP films slowly under ambient conditions and can be completely removed from the TPP film under vacuum at 35 °C. Two distinct desorption regions are observed, both following first order desorption kinetics. This is likely the result of a transition to a stronger bonding environment after half of the DMMP has been desorbed from the film. The TPP films are returned to their initial state after desorption and will resorb DMMP in a 1:1 molar ratio.

Chapter 4
Conclusions

The goal of this research was to quantitatively examine the interaction of the chemical warfare agent (CWA) simulant dimethyl methylphosphonate (DMMP) into trisilanolphenyl-POSS (TPP) Langmuir-Blodgett (LB) films. The study of the reactions of CWA simulants is important in developing improved CWA decomposition mechanisms, CWA sensors, and CWA protective coatings. As described in Chapter 1, recent studies suggest nanostructured silicon oxide based surfaces, such as TPP, may be useful in sequestering CWA simulants. TPP is composed of a hard, inorganic silicon oxide core surrounded by softer, organic phenyl groups. A quartz crystal microbalance (QCM) was used to investigate the sorption and desorption of DMMP from well-ordered thin films of TPP.

The sorption and desorption of DMMP from TPP LB-films has been quantitatively studied using a QCM. The sorption of DMMP into TPP increases linearly with the number of TPP layers. Further, DMMP binds to the TPP in a 1:1 molar ratio, or 1074 µmol of DMMP per gram of TPP LB-film. This value is actually larger than the degradation capacity of alumina-supported iron and cerium oxide surfaces, reported to be 510 µmol of DMMP per gram of metal oxide at 25 °C.[19] Furthermore, the 1:1 molar sorption ratio of TPP to DMMP is consistent with the bonding scheme proposed in the literature.[1] The DMMP desorbs from the TPP films slowly under ambient conditions and can be completely removed from the TPP film under vacuum at 35 °C. Two distinct desorption regions are observed, both following first order desorption kinetics. This is likely the result of a transition to a stronger bonding environment after half of the DMMP

has been desorbed from the film. The TPP films are returned to their initial chemical structure after desorption and will resorb DMMP in a 1:1 molar ratio. This subsequent re-sorption of DMMP suggests that DMMP does not decompose over TPP films, in agreement with the conclusions of Ferguson-McPherson *et al.*[1]

Chapter 5
Suggestions for Future Work

The quartz crystal microbalance (QCM) is a powerful technique for investigating adsorption and desorption chemistry and would be useful in further illuminating organophosphonate reactions with polyhedral oligomeric silsesquioxanes (POSS) films. Although dimethyl methylphosphonate (DMMP) is the most commonly studied chemical warfare agent (CWA) simulant, chlorinated CWA simulants, such as methyl dichlorophosphate (MDCP) and trichlorophosphate (TCP), though more dangerous, provide a better model for the reactivity of halogenated CWAs. Consequently, the QCM could be used to quantitatively determine the sorption of these CWA simulants into trisilanolphenyl-POSS (TPP) films. As these CWA simulants are known to decompose via hydrolysis reactions,[112] the QCM could be employed as a gravimetric tool to determine the decomposition products and stoichiometry.

The investigation of the desorption of CWA simulants from TPP is important in establishing the ability of TPP to effectively sequester these agents. The QCM could be used to detect desorption of the CWA simulants from the TPP film and also determine the desorption kinetics. By measuring desorption at several temperatures, an Arrhenius plot could be constructed and the desorption energy of the CWA simulant could be calculated.

The role of water is of primary importance in examining the reaction chemistry of CWA simulants, as water would be present in any sensor or protective coating. No special precautions were made in the present study to exclude water from the TPP films.

The presence of any water in the films and its role on the bonding and decomposition of the CWA simulants within the film must be determined.

Atomic force microscopy (AFM) measurements of the TPP films, both before and after CWA simulant sorption, could provide useful information concerning the topography of the POSS film. AFM studies after removal of the CWA simulant from the TPP could also provide information regarding the degradation and hence reusability of the POSS film.

The reactivity of the POSS films may be modified to promote improved adsorption, as well as decomposition, of CWA simulants. The incorporation of stronger electron-withdrawing organic groups to the POSS cage would likely increase the acidity of the silanols, promoting hydrolysis and subsequent decomposition of the CWA simulant. Metal-ion functionalized POSS films may also provide an improved sorption and decomposition pathway for these agents. Esker *et al.* has successfully incorporated metal ions, such as Cu^{2+}, within multilayered TPP-films.[111] Kepley *et al.* reported that Cu^{2+} functionalized SAMs adsorbed multilayers of CWA simulants,[36] while Lixin *et al.* reported the decomposition of DMMP over copper oxide surfaces.[113] Because the uptake of DMMP into TPP LB-films is not surface limited, as the case with most metal oxides, POSS molecules with enhanced reactivity may prove superior in sequestering and decomposing CWA simulants.

Bibliography

1. Ferguson-McPherson, M.; Low, E.; Esker, A.; Morris, J. *J. Phys. Chem. B.* **2005**, *109*, 18914.

2. Yang, Y.-C. *Acc. Chem. Rev.* **1999**, *32*, 109.

3. *Convention on the Prohibition of the Development, Production, Stockpiling and Use of Chemical Weapons and on their Destruction.* **1993**, 32 ILM 800.

4. Baier, R. W.; Weller, R. W. *Ind*. Eng. *Chem. Process Des. Dev.* **1967**, *6*, 380.

5. Yang, Y.-C.; Baker, J.A.; Ward, J.R. *Chem. Rev.* **1992**, *92*, 1729.

6. Yang, Y.-C.; Szafraniec, L.; Beaudry, W.; Rohrbaugh, D.K. *J. Am. Chem. Soc.* **1990**, *112*, 6621.

7. Wagner, G.; Bartram, P.; Koper, O.; Klabunde, K. *J. Phys. Chem. B.* **1999**, *103*, 3225.

8. Wagner, G.; Koper, O.; Lucas, E.; Decker, S.; Klabunde, K. *J. Phys. Chem. B.* **2000**, *104*, 5118.

9. Wagner, G.; Procell, R.; O'Conner, R.; Munavalli, S.; Carnes, C.; Kapoor, P.; Klabunde, K. *J. Am. Chem. Soc.* **2001**, *123*, 1636.

10. Zimmerman, C.; Mazein, P.; Rebiere, D.; Dejous, C.; Pistre, J.; Planade, R. *IEEE Sensors Journal.* **2004**, *4*, 479.

11. Templeton, M.; Weinberg, W. *J. Am. Chem. Soc.* **1985**, *107*, 774.

12. Templeton, M.; Weinberg, W. *J. Am. Chem. Soc.* **1985**, *107*, 87.

13. Aurian-Blajeni, B.; Boucher, M. *Langmuir.* **1989**, *5*, 170.

14. Mitchell, M.; Sheinker, V.; Mintz, E. *J. Phys. Chem. B.* **1997**, *101*, 11192.

15. Sheinker, V.; Mitchell, M. *Chem. Mater.* **2002**, *14*, 1257.

16. Henderson, M.; Jin, T.; White, J. *J. Phys. Chem.* **1986**, *90*, 4607.

17. Mitchell, M.; Sheinker, V.; Mintz, E. *J. Phys. Chem. B.* **1997**, *101*, 11192.

18. Tesfai, T.; Sheinker, V.; Mitchell, B. *J. Phys. Chem. B.* **1998**, *102*, 7299.

19. Mitchell, M.; Sheinker, V.; Tesfamichael, A.; Gatimu, E.; Nunley, M. *J. Phys. Chem. B.* **2003**, *107*, 580.

20. Decker, S.; Klabunde, J.; Khaleel, A.; Klabunde, K. *Environ. Sci. Technol.* **2002**, *36*, 762.

21. Lin, S-T.; Klabunde, K. *Langmuir.* **1985**, *1*, 600.

22. Li, Y-X.; Klabunde, K. *Langmuir.* **1991**, *7*, 1388.

23. Li, Y-X.; Schlup, J.; Klabunde, K. *Langmuir.* **1991**, *7*, 1394.

24. Li, Y-X.; Koper, O.; Atteya, M.; Klabunde, K. *Chem. Mater.* **1992**, *4*, 323.

25. Zhanpeisov, N.; Zhidomirov, G.; Yudanov, I.; Klabunde, K. *J. Phys. Chem.* **1994**, *98*, 10032.

26. Jiang, Y.; Decker, S.; Mohs, K.; Klabunde, K. *Journal of Catalysis.* **1998**, *180*, 24.

27. Henderson, M.; Jin, T.; White, J. *J. Phys. Chem.* **1986**, *90*, 4607.

28. Kanan, S.; Tripp, C. *Langmuir.* **2001**, *17*, 2213.

29. Kanan, S.; Tripp, C. *Langmuir.* **2002**, *18*, 722.

30. Rusu, C.; Yates, J. *J. Phys. Chem. B.* **2000**, *104,* 12292.

31. Kim, C.; Lad, R.; Tripp, C. *Sensors and Actuators B.* **2001**, *76*, 442.

32. Obee, T.; Satyapal, S. *Journal of Photochemistry and Photobiology A: Chemistry.* **1998**, *118*, 45.

33. O'Shea, K.; Beightol, S.; Garcia, I.; Aguilar, M.; Kalen, D.; Cooper, W. *Journal of Photochemistry and Photobiology A: Chemistry.* **1997**, *107*, 221.

34. Moss, J.; Szczepankiewicz, S.; Park, E.; Hoffman, M. *J. Phys. Chem. B*. **2005**, *109*, 19779.

35. Panayotov, D.; Kondratyuk, P.; Yates, J. *Langmuir*. **2004**, *20*, 3674.

36. Kepley, L.; Crooks, R.; Ricco, A. *Anal. Chem*. **1992**, *64*, 3191.

37. Crooks, R.; Yang, H.; McEllistrem, L.; Thomas, R.; Ricco, A. *Farraday Dicussions*. **1997**, *107*, 285.

38. Bertilsson, L.; Engquist, I.; Liedberg, B. *J. Phys. Chem. B*. **1997**, *101*, 6021.

39. Bertilsson, L; Kamloth, K.; Liess, H.; Engquist, I.; Liedberg, B. *J. Phys. Chem. B*. **1998**, *102*, 1260.

40. Bertilsson, L.; Kamloth, K.; Liess, H. *Langmuir*. **1999**, *15*, 1128.

41. Levitsky, I.; Krivoshlykov, S.; Grate, J. *Anal. Chem*. **2001**, *73*, 3441.

42. Zimmermann, C.; Mazein, P.; Rebiere, D.; Dejous, C.; Pistre, J.; Planade, R. *IEEE Sensors Journal*. **2004**, *4*, 479.

43. King, D. A.; Wells, M. G. *Surf. Sci*. **1972**, *29*, 454-482.

44. Buttry, D.; Ward, M. *Chem. Rev*. **1992**, *92*, 1355.

45. Marx, K. *Biomacromolecules*. **2003,** *4*, 1099.

46. Alder, J.; McCallum, J. *Analyst* **1983**, *108*, 1169.

47. Ali, Z.; Pavey, K.; Roberts, E. *Journal of Thermal Analysis and Calorimetry*. **2003**, *71*, 31.

48. O'Sullivan, C; Guilbault, G. *Biosensors & Bioelectronics*. **1999**, *14*, 663.

49. Martin, S.; Granstaff, V.; Fyre, C. *Anal. Chem*. **1991**, *63*, 2272.

50. Sauerbrey, G. *Zeitschrift fuer Physik*. **1959**, *155*, 206-222.

51. Lu, C.; Lewis, O. J. *Appl. Phys*. **1972**, *43*, 4385.

52. Vionova, M.; Jonson, M.; Kasemo, B. *Biosensors and Bioelectronics*. **2002**, *17*, 835.

53. Vionova, M.; Jonson, M.; Kasemo, B. J. Phys.: *Condens. Matter*. **1997**, *9*, 7799.

54. Moya, S.; Brown, A.; Azzaroni, O.; Huck, W. *Macromol. Rapid Commun*. **2005**, *26*, 117.

55. Glassford, A.P.M. *J. Vac. Sci. Technol.* **1978**, *15,* 1836.

56. Kanazawa, K.K; Gordon, *J. Anal Chem.* **1985**, *57*, 1770.

57. Bruckenstein, S.; Shay, M. *Electrochim. Acta.* **1985**, *30*, 1295.

58. Martin, B.A.; Hager, H.E. J. *Appl. Phys*. **1989**, *65*, 2630.

59. Schumacher, R.; Borges, G.; Kanazawa, K. *Surf. Sci.* **1985**, *163*, 621.

60. Schumacher, R.; Gordon, J.; Melroy, O. *J. Electrochem. Chem*. **1987**, *216*, 127.

61. Heusler, K.E.; Grzegorzewski, A; Jackel, L; Pietrucha, J. *Ber. Bunsen-Ges. Phys. Chem.* **1988**, *92*, 1218.

62. Vig, J.R.; Ballato, A. *Ultrasonic Instruments and Devices*. Academic Press: 1999.

63. Guilbault, G.; Jordan, J. *Critical Reviews in Anal. Chem.* **1988**, *19*, 28.

64. Ermolaeva, T.N.; Lavrent'eva, T.; Seredkin, A.; Korenman, Ya. *Russian Journal of Applied Chemistry*. **2001**, *369*, 613.

65. Benje, M.; Eiermann, M.; Pittermann, U.; Weil, K. *Ber. Bunsenges, Phys. Chem*. **1986**, *90,* 435.

66. Bourkane, S.; Gabrielli, C.; Keddam, M. *Electrochim. Acta* **1989**, *34*, 1081.

67. Auge, J.; Hauptmann, P.; Eichelbaum, F.; Rosler, S. *Sensors and Actuators B*. **1994**, *90*, 435.

68. Orata, D.; Buttry, D. *J. Am. Chem. Soc.* **1987**, *109*, 3574.

69. Bott, A. W. *Current Separations*. **1999**, *18,* 79.

70. Maramatsu, H.; Tamiya, E.; Karube, I. *Anal. Chem*. **1988**, *60,* 2142.

71. Yang, M.; Thompson, M. *Anal. Chem*. **1993**, *65*, 1158.

72. Makato, M. et al., *Anal. Chem.* **1993**, *65*, 2933.

73. Ben-Dov, I.; Willmer, I. *Anal. Chem.* **1997**, *69*, 3506.

74. Tanaka, M.; Matsugushi, M. *Chemical Sensors*. **2002**, *18*, 151.

75. Worley, C.; Linton, R. *J. Vac. Sci. Technol. A*. **1995**, *13*, 2281.

76. Ulman, A. *An Introduction to Ultrathin Organic Films: From Langmuir-Blodgett to Self-Assembly*. Academic Press: San Diego, **1991**.

77. Schreiber, F. *Progress in Surface Science.* **2000**, 65, 151.

78. Ulman, A. *Chemical Reviews*. **1996**, *96*, 1533.

79. Gooding, J.J.; Hibbert, D.B. *Trends in Analytical Chemistry*. **1999**, *18*, 525.

80. Karpovich, D.; Blanchard, G. *Langmuir*. **1997**, *13*, 4031.

81. Standford Research Systems *QCM200 Operation and Service Manual.* **2005**

82. Roberts, G., Ed. *Langmuir-Blodgett Films*. Plenum Press: New York, **1990**.

83. Honig, E.P.; Hengst, J.H.T., Den Engelson, D. *Journal of Colloid and Interface Science*. **1973**, *45*, 92.

84. Alexander, A.E.; Schulmann, J.H. *Proceedings of the Royal Society A*. **1937**, *161*, 115.

85. Naselli, C.; Rabe, J.P.; Rabolt, J.F.; Swalen, J.D. *Thin Solid Films*. **1985**, *134*, 173.

86. Gaines, G.L. *Advances in Chemistry Series*. **1975**, *144*, 338.

87. Lukes, P.J.; Petty, M.C.; Yarwood, J. *Langmuir*. **1992**, *8*, 3043.

88. Franklin, B. *Phil. Trans*. **1774**, *64*, 445.

89. Rayleigh, L.J.S. *Proceedings of the Royal Society of London*. **1890**, *47*, 364.

90. Pockels, A. *Nature*. **1891**, *43*, 437.

91. Langmuir, I. *J. Am. Chem. Soc.* **1917**, *39*, 1848.

92. Blodgett, K. B. *J Am. Chem. Soc.* **1935**, *57*, 1001.

93. Peterson, I.R. *J. Phys. D: Appl. Phys*. **1990**, *23*, 379.

94. Petty, M.C. *Langmuir-Blodgett Films, An Introduction*. Cambridge University Press: Cambridge, **1996**.

95. Kaganer, V.M.; Mohwald, H.; Dutta, P. *Reviews of Modern Physics*. **1999**, *71*, 779.

96. Durbin, M.; Malik, A.; Richter, A.; Ghaskadvi, R.; Gog, T.;, Dutta, P. *J. Chem. Phys*. **1997**, *106*, 8216.

97. Binks, B.P. *Adv. Colloid Interface Sci*. **1991**, *34*, 343.

98. Landenbur, A. *Annalen*. **1875**, *179*, 143.

99. Scott, D. W. J. *Am. Chem. Soc*. **1946**, *68*, 356.

100. Brown, J.F.; Vogt, L.H. *J. Am. Chem. Soc*. **1965**, *87*, 4313.

101. Edelman, F.T. *Agnew. Chem. Int. Ed. Engl*. **1992**, *31*, 586.

102. Lichtenhan, J.D. et al. *Comments Inorg. Chem*. **1995**, *17*, 115.

103. Tsuchida, A. et al. *Macromolecules*. **1997**, *30,* 2818.

104. Haddad, T.S.; Lichtenhan, J.D. *Macromolecules*. **1996**, *29*, 7302.

105. Hofund, G.B.; Gonzalez, R.I.; Phillips, S.H. *J. Adhes. Sci. Technol*. **2001**, *15*, 1199.

106. Xiao, S.; Nguyen, M.; Gong, X.; Cao, Y.; Wu, H; Moses, D.; Heeger, A.J. *J. Adv. Funct. Mater*. **2003**, *13*, 25.

107. Jeon, H.G.; Mather, P.T.; Haddad, T.S. *Polym. Int*. **2000**, *49*, 453.

108. Paul, R.; Esker, A.R. *Langmuir*. **2006**, *22*, 6734.

109. Karabiyik, U.; Esker, A.R. *In Proc. Annu. Meet. Adhes. Soc*. **2005**, *28*, 253.

110. Huffer, S.M.; Esker, A.R. *232nd ACS National Meeting*. San Fransico, CA. **2006**.

111. Huffer, S.M.; Dawson, K.J; Deng, J.; Esker, A.R. In *Proc. Annu. Meet. Adhes. Soc*. **2005**, *28*, 306.

112. McPherson, M.K. *PhD Dissertation.* Virginia Tech, Blacksburg, VA **2005**.

113. Lixin, C.; Segal, S.R.; Suib, S.L.; Tang, X.; Satyapal, S. *Journal of Catalysis*. **2000**, 194, 61.

Vita

Joshua Kittle graduated from Virginia Tech in 1998 with a B.S. in Chemical Engineering and a minor in Chemistry. He also commissioned as a 2nd LT in the U.S. Air Force and was stationed at the Munitions Directorate, Air Force Research Laboratory, Eglin AFB, Florida. At the Munitions Directorate, Joshua researched and developed new high energy explosives, as well as low collateral damage explosives, published several technical reports, and oversaw an annual research budget of over half a million dollars.

As his next military assignment, Joshua enrolled at Virginia Tech in August 2005 in pursuit of a M.S. in Physical Chemistry under the direction of Dr. Alan R. Esker. Following the completion of his M.S. on the sorption of chemical warfare agent (CWA) simulants into trisilanolphenyl-polyoligomeric silsesquioxane films, Joshua will serve as a chemistry instructor at the U.S. Air Force Academy in Colorado Springs, CO and plans to continue his research into CWA simulant reactions.